**Title**

Resistance to thyroid hormone mutations alter hormone association and disrupt loop one through increased structural mobility

**Permalink**

https://escholarship.org/uc/item/2cw4z7cm

**Author**

Huber, Bertrand Russell

**Publication Date**

2001

Peer reviewed|Thesis/dissertation

Resistance to Thyroid Hormone Mutations Alter Hormone association and
Disrupt Loop One through Increased Structural Mobility

by

Bertrand Russell Huber

DISSERTATION

Submitted in partial satisfaction of the requirements for the degree of
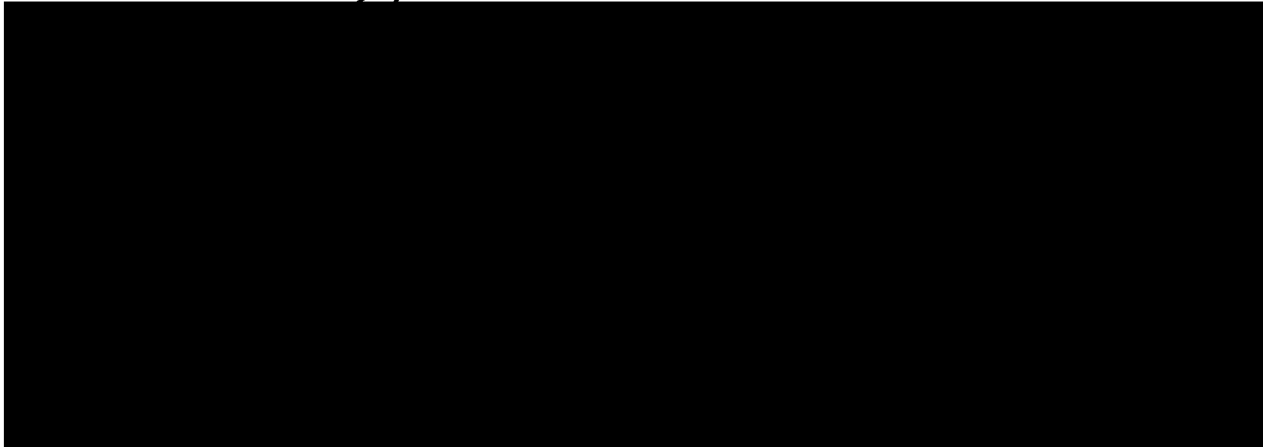
DOCTOR OF PHILOSOPHY

in

Biophysics

in the

GRADUATE DIVISION

of the

UNIVERSITY OF CALIFORNIA SAN FRANCISCO

Date ................................................................ University Librarian

Degree Conferred: ................................................................

This work is dedicated to my parents
who have encouraged my curiosity
And
To Shannon who has loved me
during the rough times

# Abstract

High levels of hormone, without the symptoms of hormone excess, generally characterize hormone resistance syndromes. Two mutations frequently found in the thyroid hormone receptor (TR) ligand binding pocket that cause resistance to thyroid hormone (RTH) are A317T and R316H. In A317T mutation the Ala 317 residue is located next to the 3' iodine of Triac. Mutation to Thr changed the position of the ligand within the pocket, introducing a packing defect in the receptor, which increased the volume of the receptor. The actual site of the mutation remained stable, forcing the ligand to shift and rotate away from the mutation into the opposite face of the receptor, which bulged out to accommodate the shift. In the R316H mutation, the Arg 316 side chain of TRβ forms three side chain hydrogen bonds within the receptor. Two of these hydrogen bonds are with Thr 232, which is part of helix 1. Both of these hydrogen bonds were eliminated as a result of the mutation. The loss of hydrogen bonds and the electrostatic change caused by the R316H mutation significantly increase mobility and $k_{off}$. Two other mutations, A234T and R243Q, occur in the flexible region of the receptor that links the DNA binding domain (DBD) and ligand binding domain (LBD.) Mutations of the hinge in TR are unusual because they cause RTH without a significant decrease in hormone binding function. Using X-ray crystallography we observed that mutations in the loop following helix one modulate the flexibility and position of this region of the LBD. The hinge mutant structures suggest that mobility in loop one causes a decoupling of hormone binding and corepressor release. Though all of these mutations disrupt the TR in unique ways. There is a general trend that RTH mutations increased structural mobility. The increased structural mobility was localized primarily to loop 1,

iv

helix 2 and loop2. All of these elements surround the ligand cavity. The degree of mobility

observed in the mutant structures correlated to some degree with the ligand off rate.

# Table of Contents

# List of Tables

# List of Figures/Illustrations

## Importance of Determining the Structures of RTH Mutants and SF-1

Resistance to thyroid hormone (RTH) syndrome decreases tissue responsiveness to thyroid hormone (3,5,3'-triiodio-L-thyronine, $T_3$) leading to an increase in circulating concentration of thyroid hormone (1). Clinically, RTH is identified by high levels of $T_3$, goiter and a generally euthyroid state. This syndrome is caused by variety of different mutations in the thyroid hormone receptor beta (TR$\beta$). The RTH point mutations present the opportunity to understand the structural basis of hormone resistance in the TR. A structural understanding of RTH will make it possible to rationally design therapeutics that mitigate specific mutations of the TR and restore hormonal balance. Moreover, elucidating the principals that govern TR function may make it possible to design ligands that take advantage of receptor ligand interactions that elicit specific responses from the TR, thus making ligands with entirely new therapeutic profiles. The structural similarity between TR and the other nuclear receptors may allow the principles described here to generalize to other member of the nuclear receptor (NR) family. We have also set out to determine the structure of Steriodogenic factor one (SF-1), which does not appear to be regulated by a cognate hormone. The preponderance of evidence suggests that SF1's transcriptional activity is modulated by phosphorylation resulting from the MAP kinase cascade. The lack of apparent hormone and unusual arrangement of SF-1 makes it an ideal protein for structural studies of nuclear receptor phosphorylation.

## Nuclear Receptor

Members of the NR's play a fundamental role in development and metabolism. Protein products encoded by these genes include receptors for thyroid hormone, steroid

2

hormones, retinoids, prostaglandins, vitamin D, fatty acids, and a group of receptors without known ligands termed orphan receptors (2-8). The nuclear hormone receptors are key transcriptional regulators, which are responsible for developmental processes ranging from sexual differentiation to neural development. The majority of the well-studied nuclear receptors have cognate hormones. However, there is some conjecture whether all of the NR's have distinct hormones.

## Characteristics of the Nuclear Receptors

The majority of known nuclear receptors share a signature sequence responsible for the interaction with DNA, referred to as the DNA binding domain (DBD or C domain). The DBD possesses two characteristic cystine containing zinc fingers (9), which are responsible for binding and recognition of cognate DNA response elements (RE). A typical RE is composed of one or more six base pair half sites. The arrangement of these half sites has an impact on the arrangement and composition of NR's, that bind to the response element(10). Nuclear receptors bind to response elements as monomers, homodimers and heterodimers.

For most receptors the DBD is preceded by an N-terminal activation domain referred to as the A/B domain or activation function one domain (AF-1). This domain is associated with ligand independent transcriptional activation in a number of receptors (11, 12). The structure of the AF-1 domain is unknown.

The DBD domain is linked to the ligand-binding domain (LBD or E domain) by a hinge region (D domain). This region was classified as a hinge because of the hormone modulated proteolytic susceptibility observed in many of the nuclear receptors (13). In the absence of hormone the hinge region has been shown to interaction with corepressors (14, 15). Structurally, the hinge region appears to be divided between the LBD and DBD (16).

3

The LBD domain forms a pocket, which completely encloses ligand. The structure of the LBD is made up of twelve helices arranged into a three layer helical sandwich, with a small region of b-sheet referred to as the b-hairpin loop (17-21). The middle of the sandwich is made up of two helices and ligand. The LBD domain also interacts with a host of coregulators that mitigate transcription.

The activation function two domain (AF-2) originally thought to be a separate structural domain maps to helix twelve of the LBD. The ligand dependant activation of AF-2 results from a structural rearrangement in the LBD resulting in a repositioning of helix 12 in response to hormone binding (18, 22, 23).

## Nuclear Receptors and MAP kinases

Nuclear receptors serve as an integration site for endocrine signals. The NR's exist as part of complex with other coregulators that modulate expression from controlled genes. Much of what is known about NR transcriptional activation has come from studies of hormonal control. However, factors other than hormone concentration mediate NR transcriptional activation. A number of nuclear receptors are physphorylated by MAP kinases or interact with other proteins that are part of a MAP kinase cascade. Both PPAR-$\gamma$ and ER appear to be linked to MAP kinase pathways directly by phosphorylation sites found within the AF-1 domain (24, 25). The effect of phosphorylation on transcription is weaker than hormone binding for these receptors. However in other receptors like steriodogenic factor one (SF-1) transcriptional activation appears to be more directly controlled by phosphorylation.

4

## Hormone Resistance in Nuclear Receptors

The nuclear receptor gene superfamily is one of the largest gene families. Protein products encoded by these genes include receptors for thyroid hormone, steroid hormones, retinoids, prostaglandins, vitamin D, fatty acids, and receptors without known ligands termed orphan receptors (2-8). Syndromes caused by defects in several of these receptors have been described. These include androgen resistance (26), glucocorticoid resistance (27), mineralocorticoid resistance (28), vitamin D resistant rickets (29), and RTH (1), which are all caused by defects in the cognate receptor. These syndromes have in common high levels of the cognate hormone with decreased responsiveness in target tissues. Continued study of NRs will invariably lead to the discovery of hormone resistance in other NR's.

## Thyroid Hormone Receptor and Retinoic Acid Receptor

The thyroid hormone receptor (TR) is an integral part of both development and metabolism. During intrauterine human development the absence of thyroid hormone leads to irreversible damage to the central nervous system. Continued deprivation of thyroid hormone leads to a condition called cretinism, which is characterized by arrested growth and decreased intelligence (30). Abnormalities in thyroid hormone levels after development have serious metabolic consequences. An excess of thyroid hormone (hyperthyroidism) causes hyperactivity, increased heart rate, tachicardia and weight loss. A deficiency of thyroid hormone (hypothyroidism) leads to lethargy, weight gain and mental depression.

The TR has been found to bind to DNA as monomer, homodimer or as a heterodimer with the retinoic acid receptor (RXR) (10). The formation of dimers is highly dependent on the RE and the ligand state of TR. The most commonly found TR response element is the

5

direct repeat four (DR4). The DR4 has two parallel six base pair TR half sites separated by four random base pairs. The consensus sequence for the TR half site is AGGTCA, which is shared with a number of the other nuclear receptors, most importantly RXR. The unliganded TR binds to the DR4 as both a homodimer or as a heterodimer with RXR (31). The addition of hormone strongly favors the formation of the heterodimer with RXR and dissociation of the homodimer (32).

RE's are found in the promoter region of TR controlled genes. Depending on the context and tissue, thyroid hormone either positive or negatively regulates transcription. In positively controlled genes the absence of ligand allows TR to bind to corepressors such as SMRT, NCOR and RIP13 (33-35), which are part of complex responsible for gene repression. The repressor complex contains histone deacetylase (36). Histone remodeling achieved with acetylases and deacetylases is thought to regulate expression of NR controlled genes (37).

Binding of $T_3$ to TR causes corepressors to dissociate and forms a hydrophobic pocket on the surface of the TR, which allows coactivator to bind (38). Coactivators appear to interact with TR through a signature LXXLL motif that binds to a hydrophobic cleft formed by helix 3, 4, 5 and 12 (38, 39). The coactivator can interact with other transcriptional activation factors such as CBP (40, 41) and components of the basil transcriptional machinery (42) to form a transcriptional activation complex. NR promoter sites generally contain more than one nuclear receptor response elements and more response elements generally correspond to higher levels of transcription from NR controlled gene (43).

## Resistance to Thyroid Hormone

Hormone resistance in the TR results from point mutations, truncations and translocations within the TR LBD as well as interactions with defective coregulators (1). RTH point mutations are autosomal dominant. Abnormal TRβ receptors interfere with the actions of the normal receptors encoded by the normal copy of the TRβ gene and the two normal copies of the TRα genes. The RTH syndrome is characterized by high circulating concentrations of thyroid hormone and decreased response to thyroid hormone in target tissues.

Point mutations of the TRβ account for more than 700 cases of RTH. All of the RTH point mutations described to date are mutations in the TRβ LBD. These mutations fall into three clusters. The first and second clusters correspond to residues 310-353 and 429-461 respectively. These two regions are separated by a putative dimer-forming surface (44). Many of the mutations in the first and second cluster occur in the hormone-binding pocket of TR and alter the affinity of the thyroid hormone through direct contact with the hormone. Others alter the stability of the receptor thus increasing the hormone off rate. Some of the RTH mutants are found on the surface of the receptor clustering around the coactivator-binding site (45). These mutations usually have a lesser effect on hormone affinity; rather they prevent coactivator from associating. The third cluster is a more recently identified region, which contains residues 234-282(46). Two of the mutations in this regions A234T and R243Q display delayed corepressor release (47). In the majority of RTH cases higher levels of hormone compensate for the defect, leading to a mostly normal state. However, in more serious cases this compensatory mechanism fails, producing symptoms of hormone excess, such as rapid heart rate and hyperactivity.

## Hormone Pocket Mutations Define the Flexible Regions of TRβ

The mutations of the TR ligand pocket used in this study were R316H and A317T(48, 49). These two mutations demonstrated how adaptable the TRβ is to steric perturbations, yet how disruptive electrostatic changes can be to the ligand-binding pocket. In the A317T mutation the larger side chain of Thr caused a deformation of the face of the receptor made up of loop one, helix two, loop two, helix three and the β-hairpin. Conversely the R316H mutant mainly altered the position of helix one. Though A317T has more concerted structural shifting; the R316H mutation has significantly lower hormone affinity. Clearly, electrostatic alteration of the receptor ligand-binding pocket was significantly more destabilizing than steric conformational shifts. The high mobility of loop one, helix two, loop two and helix three in both pocket mutations suggest that this region of the receptor was most flexible and the shifts observed in A317T would suggest that these same regions were most able to adapt to structural changes in the TR.

## Hinge Mutants Implicate Loop One in Defective Corepressor Release

Mutations found in the hinge region of the TR caused structural mobility in the loop following helix one. For both the A234T and R243Q hinge mutations(46, 47), mobility in loop one appears to decouple hormone binding from corepressor release. This suggests that loop one is somehow involved in the interaction with corepressor and that preventing loop one from tightly binding to the receptor body allows corepressor to remain associated. These two structures also show the importance of helix one in the binding of the hinge fragment. The R243Q mutation highly destabilizes loop one yet has little effect on helix one. The A234T mutation also appears to disrupt the loop one yet has little effect on the mobility of

helix one. This suggests that the interaction between helix one and the body of the receptor is stronger than the interaction between loop one the body of the receptor. Work by Pissios et al. would suggest that the binding of hinge fragment to the body of the receptor requires a ligand induced conformational shift in the body of the receptor (50). Our results would suggest that helix one was the most important structural element for association of the hinge fragment with the body of the receptor after this conformational shift has occurred.

## SF-1 Biology

Steriodogenic factor one (SF-1) is an orphan nuclear receptor responsible for the activation of genes involved in mammalian sexual differentiation and endocrine organogenesis. The Ftz-F1 gene encodes the SF-1 nuclear receptor. In mice disruption of this gene prevents the formation of adrenals, gonads and ventromedial hypothalamus as well as selected pituitary cell types (51-54). In humans the loss of one copy of the SF-1 gene leads to sex reversal and adrenal insufficiency (55) suggesting that the role of SF-1 is similar in mammalian species. SF-1 regulates key genes in sexual differentiation such as Mullerian inhibiting substance (MIS) (56, 57) and specific P450 hydoxylases (58, 59). These same hydoxylases participate the synthesis of glucocorticoids and mineralocorticoids. Thus SF-1 controls the production of both sex and adrenal steroids.

## Organization of SF-1

The SF-1 receptor is organized somewhat differently than majority of nuclear receptors. In general nuclear receptors starting with the N-terminus are organized: AF-1, DBD, hinge region, LBD and AF-2. SF-1 is unusual because the AF-1 domain is found between the hinge region and the LBD rather than proceeding the DBD. SF-1 also possesses

an exceptionally long (~100 residue) proline rich hinge region. The close proximity of the LBD and AF-1 in SF-1 offers the opportunity to obtain the crystal structure of both domains together. Such a structure might also lead to a better understanding of the role phosphorylation plays in nuclear receptor structure.

## Does SF-1 have a Ligand?

The existence of a hormone for SF-1 has not been demonstrated. One potential ligand, 25-hydroxycholesterol, activates SF-1 in CV-1 cells, but fails to activate in any other cell line (60-62). The apparent lack of a cognate ligand may be the result of rapid degradation of the ligand or that the ligand is a ubiquitous molecule. Though SF-1 may have a specific hormone or a group of low affinity ligands it is not clear that they play a role in SF-1 mediated transcriptional activation. Clearly, an X-ray crystal structure would help to determine whether SF-1 has a ligand and aid identification of the ligand if one is present. One key factor in SF-1 activation is phosphorylation. Studies of SF-1 activation have found that phosphorylation of Ser 203 strongly enhances transcriptional from SF-1 controlled genes (63). Phosphorylation is mediated by the MAP kinase Erk2. The Erk2 signaling pathway responds to signals originating at the cell surface. This is consistent with the observation that peptide hormones for GnRH, FSH and ACTH can stimulate genes with SF-1 response elements located within their the promoter regions (64-67)

10

# References

1.    Refetoff S, Weiss R, Usala S 1993 The Syndromes of Resistance to Thyroid
      Hormone. 14:348-398

2.    Carlson-Jurica M, Schrader W, O'Malley B 1990 Steroid receptor family: structure
      and function. 11:201-220

3.    Lazar MA 1993 Thyroid hormone receptors: multiple forms, multiple possibilities.
      14:184-193

4.    Mangelsdorf DJ, Thummel C, Beato M, Herrlich P, Schütz G, Umesono K, Blumberg
      B, Kastner P, Mark M, Chambon P, et al. 1995 The nuclear receptor superfamily: the
      second decade. Cell 83:835-9

5.    Beato M, Herrlich P, Schutz G 1995 Steroid hormone receptors: many actors in
      search of a plot. 83:851-858

6.    Kastner P, Mark M, Chambon P 1995 Nonsteroidal nuclear receptors: what are
      genetics telling us about their role in real life. 83:859-870

7.    Evans RM 1988 The steroid and thyroid hormone receptor superfamily. Science
      240:889-95

8.    Mangelsdorf D, Evans RM 1995 The RXR heterodimers and orphan receptors.
      83:841-850

9.    Evans RM, Hollenberg SM 1988 Zinc fingers: guilt by association. 52:1-3

10.   Glass CK 1994 Differential recognition of target genes by nuclear receptor
      monomers, dimers and hetrodimers. 15:391

11. Langlois MF, Zanger K, Monden T, Safer JD, Hollenberg AN, Wondisford FE 1997 A unique role of the beta-2 thyroid hormone receptor isoform in negative regulation by thyroid hormone. Mapping of a novel amino-terminal domain important for ligand-independent activation. J Biol Chem 272:24927-33

12. Safer JD, Langlois MF, Cohen R, Monden T, John-Hope D, Madura JP, Hollenberg AN, Wondisford FE 1997 Isoform variable action among thyroid hormone receptor mutants provides insight into pituitary resistance to thyroid hormone. 11:16-26

13. Leng X, Tsai S, O'Malley B, Tsai MJ 1993 Ligand dependent conformational changes in thyroid hormone and retinoic acid receptors are potentially enhanced by heterodimerization with retinoic X receptors. 46:643-661

14. Kurokawa R, Söderström M, Hörlein A, Halachmi S, Brown M, Rosenfeld MG, Glass CK 1995 Polarity-specific activities of retinoic acid receptors determined by a co-repressor [see comments]. Nature 377:451-4

15. Baniahmad A, Köhne AC, Renkawitz R 1992 A transferable silencing domain is present in the thyroid hormone receptor, in the v-erbA oncogene product and in the retinoic acid receptor. Embo J 11:1015-23

16. Wagner R, Huber B, Shiau A, Kelly A, Cunha-lima ST, Scanlan T, Apriletti J, Baxter JD, West BL, Fletterick RJ 2001 Hormone Selectivity in Thyroid Hormone Receptors. 15:398-410

17. Wagner RL, Apriletti JW, McGrath ME, West BL, Baxter JD, Fletterick RJ 1995 A structural role for hormone in the thyroid hormone receptor. Nature 378:690-7

18. Bourguet W, Ruff M, Chambon P, Gronemeyer H, Moras D 1995 Crystal structure of the ligand-binding domain of the human nuclear receptor RXR-alpha [see comments]. Nature 375:377-82

19. Brzozowski AM, Pike AC, Dauter Z, Hubbard RE, Bonn T, Engström O, Ohman L, Greene GL, Gustafsson JA, Carlquist M 1997 Molecular basis of agonism and antagonism in the oestrogen receptor. Nature 389:753-8

20. Nolte RT, Wisely GB, Westin S, Cobb JE, Lambert MH, Kurokawa R, Rosenfeld MG, Willson TM, Glass CK, Milburn MV 1998 Ligand binding and co-activator assembly of the peroxisome proliferator-activated receptor-gamma. Nature 395:137-43

21. Williams SP, Sigler PB 1998 Atomic structure of progesterone complexed with its receptor. Nature 393:392-6

22. Shiau AK, Barstad D, Loria PM, Cheng L, Kushner PJ, Agard DA, Greene GL 1998 The structural basis of estrogen receptor/coactivator recognition and the antagonism of this interaction by tamoxifen. Cell 95:927-37

23. Uppenberg J, Svensson C, Jaki M, Bertilsson G, Jendeberg L, Berkenstam A 1998 Crystal structure of the ligand binding domain of the human nuclear receptor PPARgamma. J Biol Chem 273:31108-12

24. Zhang B, Berger J, Zhou G, Elbrecht A, Biswas S, White-Carrington S, Szalkowski D, Moller DE 1996 Insulin- and mitogen-activated protein kinase-mediated phosphorylation and activation of peroxisome proliferator-activated receptor gamma. J Biol Chem 271:31771-4

25.     Kato S, Endoh H, Masuhiro Y, Kitamoto T, Uchiyama A, Sasaki A, Masushige S, Gotoh Y, Nishida E, Kawashima H, Metzger D, Chambon P 1995 Activation of the estrogen receptor through phosphorylation by mitogen-activated protein kinase. 270:1491-1494

26.     Pinsky L, Trifiro MA, Kaufman M, al. e 1992 Androgen resistance due to mutation of the androgen receptor. J. Clin. Invest. 90:2097-2101

27.     Hurley DM, Accili D, Stratakis CA 1991 Point mutation causing a single amino acid substitution in the hormone binding domain of the glucocorticoid receptor in familial glucocorticoid receptor in familial glucocorticoid resistance. 87:680-686

28.     Komesaroff PA, Funder JW, Fuller PJ 1994 Hormone-nuclear receptor interactions in health and disease. Mineralocorticoid resistance. Bailliere's Clin. Endocrinol. Metab. 8:333-355

29.     Kristjansson K, Rut AR, Hewison M, O'Riordan JL, Hughes MR 1993 Two mutations in the hormone binding domain of the vitamin D receptor cause tissue resistance to 1,25 dihydroxyvitamin D3. J Clin Invest 92:12-6

30.     Xue-Yi C 1994 Timing of vulnerability of the brain to iodine deficiency in endemic cretinism. 331:1739

31.     Kliewer SA, Umesono K, Mangelsdorf DJ, Evans RM 1992 Retinoid X receptor interacts with nuclear receptors in retinoic acid, thyroid hormone and vitamin D3 signalling. Nature 355:446-9

32. Yen PM, Darling DS, Carter RL, Forgione M, Umeda PK, Chin WW 1992 Triiodothyronine (T3) decreases binding to DNA by T3-receptor homodimers but not receptor-auxiliary protein heterodimers. J Biol Chem 267:3565-8

33. Seol W, Choi HS, Moore DD 1995 Isolation of proteins that interact specifically with the retinoid X receptor: two novel orphan receptors. Mol Endocrinol 9:72-85

34. Hörlein AJ, Näär AM, Heinzel T, Torchia J, Gloss B, Kurokawa R, Ryan A, Kamei Y, Söderström M, Glass CK, et al. 1995 Ligand-independent repression by the thyroid hormone receptor mediated by a nuclear receptor co-repressor [see comments]. Nature 377:397-404

35. Chen JD, Evans RM 1995 A transcriptional co-repressor that interacts with nuclear hormone receptors [see comments]. Nature 377:454-7

36. Heinzel T, Lavinsky RM, Mullen TM, Soderstrom M, Laherty CD, Torchia J, Yang WM, Brard G, Ngo SD, Davie JR, Seto E, Eisenman RN, Rose DW, Glass CK, Rosenfeld MG 1997 A complex containing N-CoR, mSin3 and histone deacetylase mediates transcriptional repression [see comments]. Nature 387:43-8

37. McEwan IJ 2000 Gene regulation through chromatin remodelling by members of the nuclear receptor superfamily. Biochem Soc Trans 28:369-73

38. Darimont BD, Wagner RL, Apriletti JW, Stallcup MR, Kushner PJ, Baxter JD, Fletterick RJ, Yamamoto KR 1998 Structure and specificity of nuclear receptor-coactivator interactions. Genes Dev 12:3343-56

39.  Heery DM, Kalkhoven E, Hoare S, Parker MG 1997 A signature motif in transcriptional co-activators mediates binding to nuclear receptors [see comments]. Nature 387:733-6

40.  Swope DL, Mueller CL, Chrivia JC 1996 CREB-binding protein activates transcription through multiple domains. J Biol Chem 271:28138-45

41.  Chakravarti D, LaMorte VJ, Nelson MC, Nakajima T, Schulman IG, Juguilon H, Montminy M, Evans RM 1996 Role of CBP/P300 in nuclear receptor signalling [see comments]. Nature 383:99-103

42.  Petty KJ, Krimkevich YI, Thomas D 1996 A TATA binding protein-associated factor functions as a coactivator for thyroid hormone receptors. Mol Endocrinol 10:1632-45

43.  Kato S, Sasaki H, Suzawa M, Masushige S, Tora L, Chambon P, Gronemeyer H 1995 Widely spaced, directly repeated PuGGTCA elements act as promiscuous enhancers for different classes of nuclear receptors. Mol Cell Biol 15:5858-67

44.  Parrilla R, Mixson AJ, McPherson JA, McClaskey JH, Weintraub BD 1991 Characterization of seven novel mutations of the c-erbA beta gene in unrelated kindreds with generalized thyroid hormone resistance. Evidence for two "hot spot" regions of the ligand binding domain. J Clin Invest 88:2123-30

45.  Feng W, Ribeiro RC, Wagner RL, Nguyen H, Apriletti JW, Fletterick RJ, Baxter JD, Kushner PJ, West BL 1998 Hormone-dependent coactivator binding to a hydrophobic cleft on nuclear receptors. Science 280:1747-9

46.  Collingwood TN, Wagner R, Matthews CH, Clifton-Bligh RJ, Gurnell M, Rajanayagam O, Agostini M, Fletterick RJ, Beck-Peccoz P, Reinhardt W, Binder G,

Ranke MB, Hermus A, Hesch RD, Lazarus J, Newrick P, Parfitt V, Raggatt P, de Zegher F, Chatterjee VK 1998 A role for helix 3 of the TRbeta ligand-binding domain in coactivator recruitment identified by characterization of a third cluster of mutations in resistance to thyroid hormone. EMBO J 17:4760-70

47.     Safer JD, Cohen RN, Hollenberg AN, Wondisford FE 1998 Defective release of corepressor by hinge mutants of the thyroid hormone receptor found in patients with resistance to thyroid hormone. J Biol Chem 273:30175-82

48.     Weiss RE, Stein MA, Duck SC, Chyna B, Phillips W, O'Brien T, Gutermuth L, Refetoff S 1994 Low intelligence but not attention deficit hyperactivity disorder is associated with resistance to thyroid hormone caused by mutation R316H in the thyroid hormone receptor beta gene. J Clin Endocrinol Metab 78:1525-8

49.     Sunthornthepvarakul T, Angsusingha K, Likitmaskul S, Ngowngarmratana S, Refetoff S 1997 Mutation in the thyroid hormone receptor beta gene (A317T) in a Thai subject with resistance to thyroid hormone. Thyroid 7:905-7

50.     Pissios P, Tzameli I, Kushner PJ, Moore DD 2000 Dynamic Stabilization of Nuclear Receptor Ligand Binding Domains by Hormone or Corepressor Binding. 6:245-253

51.     Ingraham HA, Lala DS, Ikeda Y, Luo X, Shen WH, Nachtigal MW, Abbud R, Nilson JH, Parker KL 1994 The nuclear receptor steroidogenic factor 1 acts at multiple levels of the reproductive axis. Genes Dev 8:2302-12

52.     Luo X, Ikeda Y, Parker KL 1994 A cell-specific nuclear receptor is essential for adrenal and gonadal development and sexual differentiation. 481-490

53.  Sadovsky Y, Crawford PA, Woodson KG, Polish JA, Clements MA, Tourtellotte LM, Simburger K, Milbrandt J 1995 Mice deficient in the orphan receptor steroidogenic factor 1 lack adrenal glands and gonads but express P450 side-chain-cleavage enzyme in the placenta and have normal embryonic serum levels of corticosteroids. Proc Natl Acad Sci U S A 92:10939-43

54.  Shinoda K, Lei H, Yoshii H, Nomura M, Nagano M, Shiba H, Sasaki H, Osawa Y, Ninomiya Y, Niwa O, et al. 1995 Developmental defects of the ventromedial hypothalamic nucleus and pituitary gonadotroph in the Ftz-F1 disrupted mice. Dev Dyn 204:22-9

55.  Achermann JC, Ito M, Hindmarsh PC, Jameson JL 1999 A mutation in the gene encoding steroidogenic factor-1 causes XY sex reversal and adrenal failure in humans [letter]. Nat Genet 22:125-6

56.  Giuili G, Shen WH, Ingraham HA 1997 The nuclear receptor SF-1 mediates sexually dimorphic expression of Mullerian Inhibiting Substance, in vivo. Development 124:1799-807

57.  Shen WH, Moore CC, Ikeda Y, Parker KL, Ingraham HA 1994 Nuclear receptor steroidogenic factor 1 regulates the müllerian inhibiting substance gene: a link to the sex determination cascade. Cell 77:651-61

58.  Morohashi K, Zanger UM, Honda S, Hara M, Waterman MR, Omura T 1993 Activation of CYP11A and CYP11B gene promoters by the steroidogenic cell-specific transcription factor, Ad4BP. Mol Endocrinol 7:1196-204

59.     Rice D, Kronenberg H, Mouw AR, Aitken A, Franklin BP, Schimmer BP, Parker K 1990 Multiple regulatory elements determine adrenocortical expression of steroid 21-hydroxylase. 265:8052-8058

60.     Christenson LK, McAllister JM, Martin KO, Javitt NB, Osborne TF, Strauss JF, 3rd 1998 Oxysterol regulation of steroidogenic acute regulatory protein gene expression. Structural specificity and transcriptional and posttranscriptional actions. J Biol Chem 273:30729-35

61.     Lala DS, Syka PM, Lazarchik SB, Mangelsdorf DJ, Parker KL, Heyman RA 1997 Activation of the orphan nuclear receptor steroidogenic factor 1 by oxysterols. Proc Natl Acad Sci U S A 94:4895-900

62.     Mellon SH, Bair SR 1998 25-Hydroxycholesterol is not a ligand for the orphan nuclear receptor steroidogenic factor-1 (SF-1). Endocrinology 139:3026-9

63.     Hammer GD, Krylova I, Zhang Y, Darimont BD, Simpson K, Weigel NL, Ingraham HA 1999 Phosphorylation of the nuclear receptor SF-1 modulates cofactor recruitment: integration of hormone signaling in reproduction and stress. Mol Cell 3:521-6

64.     Kaiser UB, Conn P, Chin WW 1997 Studies of gonadotropin-releasing hormone (GnRH) action using GnRH receptor expressing cell lines. 18:46-70

65.     Liu Z, Simpson ER 1997 Steroidogenic factor 1 (SF-1) and SP1 are required for regulation of bovine CYP11A gene expression in bovine luteal cells and adrenal Y1 cells. Mol Endocrinol 11:127-37

66.  Sugawara T, Holt JA, Kiriakidou M, Strauss JF, 3rd 1996 Steroidogenic factor 1-dependent promoter activity of the human steroidogenic acute regulatory protein (StAR) gene. Biochemistry 35:9052-9

67.  Wilson TE, Fahrner TJ, Milbrandt J 1993 The orphan receptors NGFI-B and steroidogenic factor 1 establish monomer binding as a third paradigm of nuclear receptor-DNA interaction. Mol Cell Biol 13:5794-804

# Chapter 1: Natural Mutations of the Thyroid Hormone Receptor Alter Receptor Binding Association through Increased Mobility of the Hormone Binding Pocket

## Introduction

Endocrinologists traditionally viewed disease states as arising from too much or too little of a hormone, and most of the classical endocrine diseases reflect states of excess or deficiency. Now, there is general awareness that alterations in sensitivity to hormones play a major role in disease, and a number of hormone resistance syndromes have been described in increasing molecular detail. Some of these syndromes are caused by mutations in genes that encode receptors for the hormones; others are caused by post-receptor defects that arise from the macromolecular interactions of the receptor. In about half of all clinical cases molecular mechanisms have eluded investigators.

Nuclear receptors are encoded by a large gene superfamily and they bind a diversity of ligands, including thyroid hormone, steroid hormones, retinoids, prostaglandins, vitamin D, fatty acids, and other ligands (1-6). Ligands for several members of the nuclear receptor family have not been identified and these are termed orphan receptors (7). Syndromes caused by defects in several nuclear receptors have been described. These include androgen resistance (8), glucocorticoid resistance (9), mineralocorticoid resistance (10), vitamin D resistant rickets (11), and resistance to thyroid hormone (RTH)(12), each caused by mutations in the appropriate receptor. These syndromes have in common high levels of the cognate hormone with decreased hormone response in target tissues.

RTH has been discovered in over 700 cases, and is characterized by high triiodothyronine, $T_3$ levels. Normally $T_3$ concentration is supported by the action of thyroid stimulating hormone (TSH), and the TSH concentration is regulated as a negative feedback mechanism. RTH is caused by mutations in the gene encoding the thyroid hormone receptor-

β (TRβ). The syndrome is autosomal dominant, and the abnormal receptors interfere with the actions of the normal receptors encoded by the normal TRβ gene and by the two alleles of the other gene that encodes the TR, TRα gene. All of the defects described to date are mutations in the TR ligand-binding domain (LBD.) This domain interacts with perhaps 20 molecules including corepressors, coactivators, and other nuclear receptors. Most of the mutated receptors have impaired binding of thyroid hormone (3,5,3'-triiodio-L-thyronine, $T_3$). However, in number of cases hormone binding is normal and some other function of the receptor has been disrupted, such as coactivator binding (13) or corepressor release (14). In many RTH cases slightly higher levels of hormone compensate for the defect, leading to a mostly normal state. However, in more serious cases resistance levels can cause mental retardation at birth, and hormone levels can rise to produce symptoms of hormone excess, such as rapid heart rate and hyperactivity.

Insights into mechanisms by which mutations in the TRβ impair receptor function were obtained from the determination of a model of the TRβ LBD based on the X-ray crystallographic structure of the rat TRα LBD (15) and subsequently that of the human TRβ (16). Prior to the availability of this data, it was observed that the mutations clustered in three separate regions of the hTRβ LBD linear sequence, but the crystallographic and modeling data indicated that the mutations mostly cluster to surround the receptor's ligand-binding cavity (17-21). Thus explaining why ligand binding is commonly impaired. Similarly, the finding that the mutations were located in regions of the receptor LBD associated with other receptor functions was consistent with the spectrum of functional defects observed in RTH. These are the only crystallographic structures of nuclear receptors with clinically relevant

mutations that have been determined to date. Thus, the syndrome is useful as a model to examine hormone resistance in general.

Whereas placement of the mutations suggests how the mutations could cause the defect, actual knowledge of the mechanism of the impairment requires knowledge of the atomic structure of the mutated receptor. In this regard the atomic structure of a mutated receptor causing a disease has never been reported for any hormone. In the current studies, we report the X-ray crystal structures of the TR mutants, R316H (22) and A317T (23). Though both of these adjacent residues are located in the hormone-binding pocket, they differ significantly in the way that they affect the receptor when mutated.

## Results

### Overall view of the structures

The mutant hTRβ LBD's for A317T and R316H were purified in the presence of Triac and crystals were obtained and analyzed by X-ray diffraction as described in Materials and Methods. The Statistics from data collection and analysis for these mutants are summarized in Table 1-1. Both mutants were similar to the native structure with an overall RMSD of positional change in atomic coordinates of 0.56 Å and 0.62 Å for A317T and R316H respectively with experimental error expected to be about 0.3 Å. The higher RMSD in R316H is consistent with the higher B-factors observed in this mutant. As observed for all members of the nuclear receptor family the fold is composed primarily of twelve helices in a three-layer a-helical sandwich. The top of the receptor in figure 1-1a is the hydrophobic core of the protein, while the bottom of the receptor is the ligand-binding pocket. Both structures also included helix 0, which is part of the link to the DNA-binding domain (DBD).

### Ligand position in the A317T pocket

Ala 317 is located in the interior of the ligand-binding cavity of the thyroid hormone receptor. Mutation of Ala 317 to Thr replaced two hydrogens with oxygen and a methyl group. The Thr 317 side chain was in Van der Waal contact with the iodine at position 3 of Triac as seen in figure 1-2. Contact distance between Thr 317 and iodine was 3.6 Å, compared to 4.1 Å for Ala 317. The terminal methyl groups of Thr 317 fits into a grove formed by the second carbon of the first phenyl ring and the iodine attached to the third carbon of the first phenyl ring of Triac. The ligand shifted away from the mutation, by 0.3 Å

25

with the hydroxyl end of the ligand rotating away from the mutation site 0.5 Å. The contacts between the ligand and the receptor observed in the wild type TRβ (16) were conserved in the mutant structure. However, the ligand-binding pocket was deformed by about 0.3 Å to 0.5 Å on the side opposite to the mutation to accommodate the mutation without disrupting the other ligand contacts.

**Affect of R316H mutation on hydrogen bonding**

The mutation of Arg 316 to His changed the hydrogen-bonding configuration of the side chain. In the native structure Arg makes three hydrogen bonds. One of these hydrogen bonds is with Gln 374, which is part of helix 9. The other two hydrogen bonds are with Thr 232, which is part of helix 1. In the mutant structure His only formed a hydrogen bond with Gln 374 and could no longer form hydrogen bonds with Thr 232. Thus the mutation freed helix 1 from hydrogen bonding with residue 316. This change in hydrogen bonding between the native and R316H mutant can be seen in figures 1-3a and 1-3b. The position of the ligand with its pocket was unchanged.

**Packing defects in the receptor opposite the A317T mutation**

The volume of the A317T receptor cavity was slightly smaller than that of the native TR by ~10 Å$^3$. This was caused by tighter packing around the ligand as a result of the 0.3 Å shift in the ligand position and the larger size of the mutant side chain. In contrast the overall volume of the A317T receptor LBD increases by ~300 Å$^3$ as a result of the new packing arrangement. Curiously, helix 6, which contains residue 317, shifted only minimally (ca 0.2Å), and helices of the receptor hydrophobic core remained relatively stable (0.3Å shift). Instead, difference distance analysis of the mutant structure verses the wild type structure

indicated that the expansion of the receptor took place primarily on the side of the receptor opposite the mutation site, where helix 3 shifted ~1 Å. The other areas that deformed to accommodate the mutation in this region were the loop between helix 1 and helix 2 (1Å) and the β-hairpin loop (1Å) Finally, a shift on the opposite side of the receptor was also observed in the loop between helix 11 and helix 12 (1Å). These shifts are shown in figure 1-4a.

## Shift in Helix one in the R316H Mutant

The R316H structure lacked the concerted one-sided expansion observed in the A317T mutant. Instead, most of the positional shift was observed in helix 1, which lost two hydrogen bonds with the body of the receptor as a result of the R316H mutation. This structural element shifted away from the body of the receptor with an RMSD of 1.0 Å. Concerted positional shifting was observed both in the section of helix 1 that interacted with Arg 316 in the native structure as well as the region of helix 1 linked to helix 0, which shifted with an RMSD of 1.1Å. A small portion of helix 3 adjacent to helix 1 shifted an RMSD of 0.82 Å away from the native position. Loop 11 also showed a significant RMSD shift of 2.0Å. This loop forms a crystal contact. The large shift observed in this region was likely due to an alteration in the crystal contacts, which would alter crystal lattice constants. These changes in the R316H structure resulted in an expansion of the receptor by ~200 $Å^3$. However, the small overall expansion of the receptor did not affect the volume of the ligand-binding pocket. These shifts are shown in figure 1-4b.

## B-factor comparison of native, A317T and R316H

The average B-factors observed in the A317T mutant structure were ~ 0.2 $Å^2$ lower than the in the native structure, which could be explained by the higher resolution and

precision of the structure determined for the mutant receptor (2.4 Å vs. 2.5 Å for the wild type receptor) or simply be the result of the unique diffraction properties of each crystal. However, two areas of the mutant receptor, loop 1 and loop 11, exhibited significantly higher relative B-factors. Helix 12 showed little change in relative B-factor between mutant and native structure (see Figure 1-5b).

Overall the R316H mutant had B-factors that were 27.2 $Å^3$ higher than that of the native structure. The R316H structure showed exceptionally high B-factors throughout helix 0, the loop following helix 0 and continuing into helix 3, the $\beta$-hairpin loop and loop 11 (figure 1-5c). These regions of high B-factors (with the exception of the $\beta$-hairpin loop) corresponded to the same regions that had high B-factors in the A317T structure. When one compared relative B-factors, these areas were much more positionally dispersed in R316H than in either the native or A317T mutant. The combination of small structural shifts with high B-factors observed in regions of these mutant structures indicated structural flexibility and mobility rather than conformational rearrangement.

## Ligand binding analysis of A317T and R316H

Ligand binding assays for the native receptor, A317T and R316H were performed with T3 to determine the ligand on rate ($k_{on}$), ligand off rate ($k_{off}$) and dissociation constant ($K_d$). For the native TR and A317T mutants the hormone dissociation constants were in agreement with previous studies. However, the dissociation constant for R316H was significantly different from previous studies (see Table 2). Our data showed that R316H binds hormone with a higher than expected affinity. The $K_d$ for R316H was much closer to the A317T mutant. These assays also showed that the kinetic parameter that changed the

most was $k_{off}$, while $k_{on}$ remained essentially diffusion controlled for both the native and mutant TR's. This data is summarized in Table 2.

## Electrostatic Alteration in the R316H mutant

The R316H mutation causes significant change in the electrostatic potential of the TR. The Arg side chain is a highly basic moiety. In the context of the folded hTRβ structure, its positive potential as seen in figure 1-6a is sandwiched between two regions of negative potential. The mutation R316H disrupts this balance by removing the basic Arg and replacing it with a neutral His. The positive electrostatic potential in the region of the His drops near the side chain and splits the large region of positive electrostatic potential observed in the native structure into two smaller regions of positive electrostatic potential. Overall the result was less positive electrostatic potential in the region of the mutation as seen in figure 1-6b.

## Discussion

These studies reveal the X-ray crystal structure of two mutated receptors implicated in RTH. These mutations are found next to one another is sequence, yet are different in the manner that they influence receptor structure and in their clinical manifestation. One of the identifiers of RTH is increased concentration of free $T_4$. For many of the RTH mutants there appears to be an inverse correlation between free hormone concentration and receptor hormone association constants. Mutants that are within two standard deviations of this trend are referred to as group one mutants (24). Mutations that do not fit the trend are referred to as group two mutants. By this definition A317T and R316H are of different classes. The A317T mutation is a prime example of a group one mutation. This mutation lies near the free

29

T$_4$ vs. hormone binding trend line. In contrast the R316H mutation is well outside of two standard deviations from this trend. Given the association constant of R316H it would be expected that free T$_4$ concentrations would be higher. This suggests that some other factor plays a role in the syndrome caused by this mutation.

**Flexible Face of hTRβ**

The mutated side chain of A317T pushes against the phenolic inner ring of the ligand. This moves the ligand and the helix 6 harboring the mutation only slightly (0.3 Å), and has only a minimal effect on the hydrophobic core of the protein. However, the movement of the ligand causes a deformation of the ligand-binding pocket, forcing it into a more tightly packed arrangement around the ligand. The receptor must pack around the new ligand position, introducing stress into the structural elements that make up part of the ligand-binding pocket, which results in an expansion of the receptor LBD. The expansion increases the overall volume of the mutant receptor LBD by ~300 Å$^3$. The receptor adapted to the ligand shift by displacing the opposite face of the receptor. Thus, suggesting that the region of the receptor, which harbors the mutation, is structurally stable and lacks the flexibility that is observed in the loops and β-sheet on the opposite face of the ligand-binding pocket. Further the results define the more flexible structural elements in the LBD as being loop 1, helix 2 (1Å), loop 2 (1Å), the beta hairpin (1Å) and the loop between helix 11 and helix 12 (1Å). The structure of A317T would suggest that H5, helix 6, helix 11 and the α-helices that are not part of the ligand-binding pocket represent a structurally stable scaffold upon which the ligand and the rest of the ligand-binding pocket fold. The flexible front face of the receptor is made up of helix 1, helix 2, helix 3 and helix 12. This face also likely rearranges

to bind coactivator and corepressor (ref). The shifts in structural elements for this mutant are consistent with a model where the front face, which binds coactivator and corepressor, is dynamically flexible.

## A317T Mutation Introduced a Packing Defect

These movements overall appear to result in a receptor structure that is less compact. The comparison of B-factors between the A317T mutation and the native structure indicate that less compact fold also results in increased mobility. Of the four regions that show a significant positional shift all but the β-hairpin loop also show increased B-factors indicating higher mobility of these structural elements. Interestingly, the β-hairpin loop is shifted in position, but exhibits near native B-factors. This is likely because the β-hairpin is buried under the loops following helix 1. However, the altered position of the ligand causes a packing defect that prevents certain structural elements from reaching the native position. This destabilizes the loops surrounding the ligand-binding cavity.

## R316H Destabilizes Helix One

The R316H mutant has a higher RMSD than A317T. However, most of these shifts appeared to be random noise caused by increased overall mobility in the receptor rather than a concerted structural rearrangement. The exception to this was in the section of helix 1 that normally would interact with Arg 316 in the native structure. This region of the receptor made a concerted shift away from His 316, with which it could no longer form hydrogen bonds. There was also a small section of helix 2, which was adjacent to helix 1 that shifted away from the body of the receptor as a result of the R316H mutation. This was likely mediated by the structural contacts between helix 1 and helix 2. Another notable shift in the

31

structure of R316H was in the position of helix 0 leading into helix 1. This area changed position probably in response to the shift in the terminus of helix 1. Loop 11 changes position significantly although this appears to be the result of packing forces. The R316H mutation likely destabilized the TR both by altering the electrostatic potential in the mutated region of the hormone and by eliminating two hydrogen bonds with helix 1. This led to enhanced mobility of the helix 1 and the regions connected to helix 1 demonstrated by the increased relative B-factors. The R316H mutation showed that regions with high B-factors expand and encompass significantly more of the receptor relative to both the A317T and native structures. Positional variation is evident primarily on one face of the receptor further supporting the assertion that there is a flexible region of the receptor LBD. This results in an increased ligand $k_{off}$.

## RTH Mutations Increase Ligand Off Rate

There appears to be a correlation between increased relative B-factors and ligand off rate. Both A317T and R316H showed increased relative B-factors in the loop following helix 1 continuing into helix 3 and in the loop following helix 11. This effect was clearly stronger in the R316H mutant than in A317T. The R316H mutant also had a higher ligand off rate than the A317T mutant. Thus there was a correlation between structural mobility and ligand off rate. It is also important to recognize that the ligand on rates were close to the diffusion-controlled limit for both mutations and similar to that of the native structure. High structural mobility indicates that elements of the receptor were sampling a larger number of conformations. It appears that the increased structural mobility did not prevent the ligand from finding and associating with receptor binding pocket. Instead, the flexibility allowed the hormone to escape the receptor-binding pocket more easily. The binding constants of

these two mutations suggest the R316H had a stronger negative affect on hormone association. The loss of two hydrogen bonds with helix 1 was clearly important. However, this mutation also changed the electrostatics in the region of the mutation. The interplay between the loss of two hydrogen bonds and the loss of charge led to high thermal mobility in R316H.

## Mutations Affect on Dimer Formation

All previous references to the A317T mutation indicate that the hormone receptor forms homodimers and heterodimers normally if lower hormone affinity is compensated for. The structure of A317T supports the hypothesis that the putative dimer-forming surface was unaltered by the mutation. This region of the receptor exhibited less than average positional shifts when compared to the rest of the structure.

This was not the case with R316H. This mutation has been shown to form heterodimers but not homodimers (25). We observe that the position of the putative dimer forming surface described by Forman et al. (26) is unaltered in the mutant structure and relative B-factors are similar to the native structure. This supports the hypothesis that the formation of heterodimers is normal in the R316H mutant. It also may imply that some aspect of the homodimer forming surface is associated with the destabilized regions of the receptor, namely two LBD's in contact with their respective DBD domains through dynamically unstable helix 1's might readily dissociate. It is not immediately apparent why this mutation fails increase free $T_4$ concentrations to a level that is consistent with its hormone binding constant. The instability of the receptor most likely plays some role. Perhaps the inability to form homodimers prevents R316H from occupying certain response

elements, or the instability of the receptor increases the probability of proteolytic degradation. Clearly more study will be needed to answer this question.

### Helix One Interaction with Receptor Body is Flexible

Two recent studies of nuclear hormone receptors examine receptor stability. Binding of helix 1 to the body of the receptor LBD is modulated by hormone and corepressors as described by work by Pissios et al (27). Structural shifts observed in A317T demonstrate that displacing the hormone also translates into a shift in helix 1. These two observations are consistent with helix 1 loosely associating with the unliganded receptor and then folding into place when ligand is present. Recent data from the NMR structure of PPAR would suggest that both the terminal of helix 1 and the loop region following helix 1 are mobile in solution (28). In fact it appears that the PPAR receptor is in some type of partial molten globule state, where most of the ligand-binding pocket is disordered. The addition of hormone to PPAR allows the receptor to complete folding and form remaining helical structural elements. This type of model is consistent with the deformations observed in the A317T mutant. The majority of the structural shifts are observed in the secondary structural elements that form part of the ligand-binding pocket.

### Materials and Methods

### Vectors

Mutant hTRβ LBD extending from residue E202 to the C-terminal residue D461 was expressed in E. Coli as a His-tagged fusion protein using the vector, pET28a (Novagen). This vector was created by removing the PstI-BamHI fragments of the pET28 TRβ E202 WT

vector (16) and replacing with the PstI-BamHI fragments from the mutated TRs derived from pCDNA vectors (gift of S. Refetoff).

## Protein expression

Mutant hTRβ LBD was expressed in E. coli strain BL21DE3 pLysS (Novagen). After growth in 2X concentrated Lennox broth (Sigma) at 22 C to an $OD_{600}$=1.5, 0.5mM isopropyl β-D thiogalactoside (IPTG, sigma) was added and growth continued for 6h. Cells were harvested by centrifugation and pellets were frozen in liquid N2 and stored at –80 C.

## Purification

Thawed pellets from 1 L culture were lysed in For TR LBD, 50 mM sodium-phosphate pH 8.0, 300 mM NaCl, 10% glycerol, 0.1% monothioglycerol, 1 mM PMSF, 1 mM Benzamidine HCl, with 0.2 mg/ml lysozyme (20 min, 0°C). Extracts were sonicated briefly to break DNA, and centrifuged (Ti45, 36000 rpm, 1h, 4°C). Load lysate on Talon resin (Clontech) equilibrated in sodium phosphate buffer, eluted with 0-300 mM imidazole gradient. Isolation of liganded (3,3', 5-triiodo-L-acetic acid (Triac; Sigma)) receptor using TSK-phenyl HPLC (TosoHaas, Philadelphia) was performed as described (29); *yield* was 3 mg/L bacterial culture. For crystallization, hTR β LBD was diluted into 20 mM Hepes pH 8.0, 3 mM DTT and concentrated to 11.5 mg/ml by ultrafiltration (Millipore UFV2BGC10). The N-terminal His-tag was not removed prior to crystallization.

## Ligand-Binding Saturation Assays

The affinities of binding of [$^{125}$I]T$_3$ to the hTRβ LBD (WT and mutants) were determined using saturation binding assays as described (16).

## Ligand-Binding Kinetic Assays

For the dissociation experiments, 1nM of $[^{125}I]T_3$ was allowed to bind 10 femtomoles

of each receptor, at $4^0C$, until they have reached equilibrium (12 hours). At that point, further

binding of radioligand to the receptors was blocked by adding unlabeled ligand, in a

concentration 100 times higher (100nM). The receptor-bound $[^{125}I]T_3$ was isolated by gravity

flow through a 2mL course Sephadex G-25 (Pharmacia Biotech) column, and quantified

using a gamma-counter (COBRA, Packard Instruments, Meriden, CT). Binding curves were

fit by nonlinear regression and the $K_{off}$ values were calculated using the one phase

exponential decay equation contained in Prism 3.0 program. The association experiments

were performed using 2nM of $[^{125}I]T_3$ and 10 femtomoles of receptor, at $4^0C$. After adding

the receptor to the ligand, specific binding was measured immediately and at various times

thereafter. 100uL was applied to coarse Sephadex G-25 column at each time and the eluate

containing the bound receptor was quantified using a gamma-counter. Binding curves were

fit by nonlinear regression and value of $K_{ob}$ determined by fitting an exponential association

equation to the data. To calculate the association rate constant ($K_{on}$), expressed in units of

Molar-1 min-1, this equation was used: $k_{on} = (k_{ob} - k_{off}) / [radioligand]$. The $K_{on}$ obtained

experimentally was compared to the expected $K_{on}$, calculated according to the law of mass

action equation: $K_d = k_{off} / k_{on}$.

## Crystallization and Preparation for Analysis

**hTRβ A317T.** Initial crystals of the A317T mutant bound to Triac were found using

the previously established conditions for the TRβ E202 histidine-tagged construct (16).

Optimization of crystallization conditions resulted in a well buffer of 700mM sodium acetate

(NaH3OAc), 200mM sodium succinate (NaSuc) and 100mM sodium cacodylate (NaCac) adjusted to pH 7.2. Crystals were flash frozen in liquid nitrogen after gradually increasing the glycerol concentration through a series of soaks. The cryo solvents contained 900mM NaH3OAc, 200mM NaSuc, 100mM NaCac and a range of glycerol concentrations from 5% to 25% in five equal steps. These crystals diffracted to 2.4Å at the Stanford Synchrotron Radiation Laboratory (SSRL) 7-1 beam line with a Mar 345 detector.

**hTRβ R316H.** The R316H mutant crystallized in the same conditions found for native hTRβ E202. Refinement of crystallization conditions produced optimal crystals at 800mM NaH3OAc and 100mM NaCac adjusted to pH 7.6. Freezing the protein for storage prior to crystallization reduced the resolution of the resulting crystals. The combination of micro seeding with TRβ/T3 crystals, fresh unfrozen protein and optimal growth conditions yielded one crystal that diffracted to 2.4Å. Cryosolvent was the same as the mother liquor with 200mM NaH3OAc added and a range of glycerol from 5% to 25% in five equal steps. One R316H Crystal diffracted to 2.4Å at the advanced light source (ALS) beamline 5.0.2. with an ADSC detector.

## Structural Refinement

**hTRβ A317T.** A data set for A317T was collected using one-degree oscillations through 120 degrees. The data set was found to be 93.3% complete to 2.4Å resolution. Crystals of A317T / Triac exhibited the same hexagonal bipyramidal morphology found in wild type receptor. Crystals displayed space group $P3_121$ (a=68.954 Å, c=131.4 Å). Reflections were indexed and scaled using DENZO and SCALEPACK (30). A molecular replacement solution was found with a Crystallography and NMR System 1.0 (31) (CNS 1.0)

rotational search using the wild type TR-β / Triac structure with ligand and mutation region omitted. The structure was refined with multiple rounds of simulated annealing using CNS 1.0 and manual rebuilding with the Quanta98 software package. Electron density maps and coordinates were managed with the Collaborative Crystallography Project Number Four in Protein crystallography package (CCP4)(32). A ten cycle round of refinement was performed with REFMAC using a matrix weight of 0.1 resulting in a final model with an R factor of 22.2% and an R-free of 25.9%.

**hTRβ R316H**. A data set of R316H was collected using one-degree oscillations through 180 degrees. This data set exhibited the same space group and morphology as the native data set. The crystal constants were slightly different (a=67.274, c=130.121). The data set for this mutant was reduced with DENZO. A simple rotational search with CNS 1.0 failed to produce an adequate molecular replacement solution. An independent molecular replacement search was performed with EPMR (33). The search converged on an acceptable solution after two rounds. The structure was refined using the same method described for A317T. However, the resulting model, with an R factor of 25.2% and a Free R of 30.2% was less well defined. An analysis of the structure showed a number of loop regions in the molecule that were highly mobile and complicated the refinement. These regions could not be represented adequately using isotropic B-factors yet showed sufficient electron density to prevent removal from the final model. We are confident that the molecular replacement solution was the correct one and the refinement was limited by the mobility of the loops. The best crystals for either mutant had a smallest dimension of 200um

38

## Data collection

| Data set | Resolution (Å) | Reflections | | Coverage (%) | *$R_{sym}$ |
|---|---|---|---|---|---|
| | | measured | unique | | |
| hTRß R316H | 3.1 | 80196 | 6382 | 96.68 | 0.051 |
| hTRß A317T | 2.4 | 54104 | 13799 | 93.3 | 0.055 |

## Refinement

| Data set | Resolution Å | Reflections | §R | §$R_{free}$ | Rms bonds | Rms Angles |
|---|---|---|---|---|---|---|
| hTRß R316H | 3.1 Å | 5699 | 25.1 % | 30.2 % | 0.004 | 1.69 |
| hTRß A317T | 2.4 Å | 12403 | 22.2 % | 25.9 % | 0.008 | 1.61 |

**$R_{sym}= \Sigma_h \; \Sigma_i \mid I_{h,i} - <I_h> \mid /\Sigma \, I_h$ for the intensity ($I$) of $i$ observations of reflection $h$.

§R factor $= \Sigma \mid F_{obs} - F_{calc} \mid / \; \Sigma \mid F_{obs} \mid$. $R_{free}$ is calculated the same as the R factor, using 10% of the reflections that were set aside for cross validation and not used in refinement.

Table 1-1: Statistics from X-ray data collection and Refinement of R316H and A317T

| Receptor | $K_d$ (Molar) | $K_{off}$ (min-1) | $K_{on}$ ($M^{-1}.min^{-1}$) |
|----------|----------------|--------------------|-------------------------------|
| Wild Type | $5.7 \times 10^{-11}$ (+- 5.0) | 0.0043 (+- 0.0008) | $4.2 \times 10^8$ (+- 0.12) |
| A317T | $4.7 \times 10^{-9}$ (+- 0.9) | 0.379 (+- 0.11) | $5.4 \times 10^8$ (+- 0.7) |
| R316H | $2.0 \times 10^{-9}$ (+- 0.3) | 0.373 (+- 0.12) | $4.4 \times 10^8$ (+- 0.5) |

Table 1-2: Receptor hormone association ($k_{on}$), dissociation ($k_{off}$) and equilibrium constants

(Kq) for $T_3$
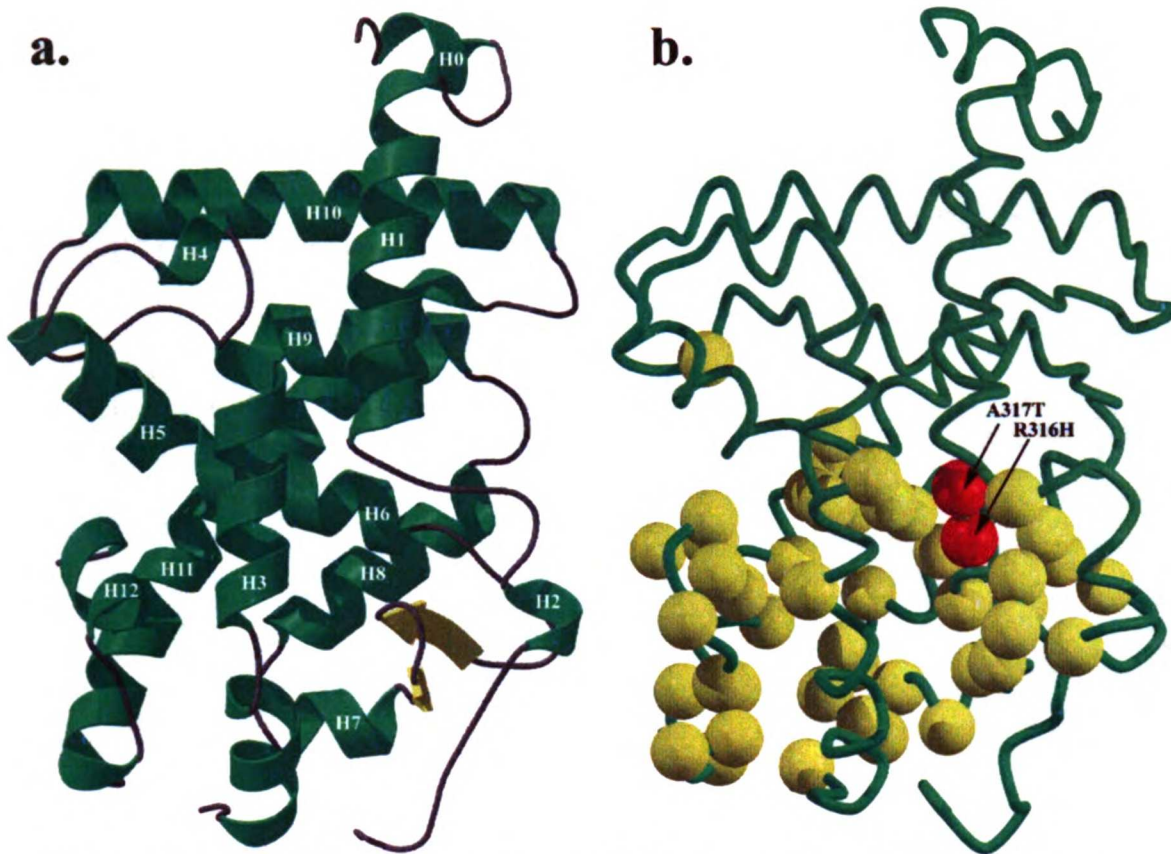
**Figure 1-1: Thyroid hormone receptor and the cluster three RTH mutations.**

a. Fold of the thyroid hormone receptor. In this schematic the structural elements of the thyroid hormone receptor beta are displayed in ribbon representation. The twelve α-helices of the TR, helix 0 and loops have been colored green. A small region of β-sheet is observed in residues 327 to 336 is colored yellow. This structural element is known as the β-hairpin loop. The omega loop, which follows helix 2 and continues to helix 3 is only partially visible in our model. The unresolved region is represented as a dashed line. b. Locations of the RTH mutations including A317T and R316H. A coil representation of the TR has been used to depict the positions of the known RTH point mutations. The positions of the RTH mutations are represented as spheres. Truncation and deletion mutations have not been included. The A317T and R316H mutations are colored yellow. The remaining structural elements in the diagram are colored gray.
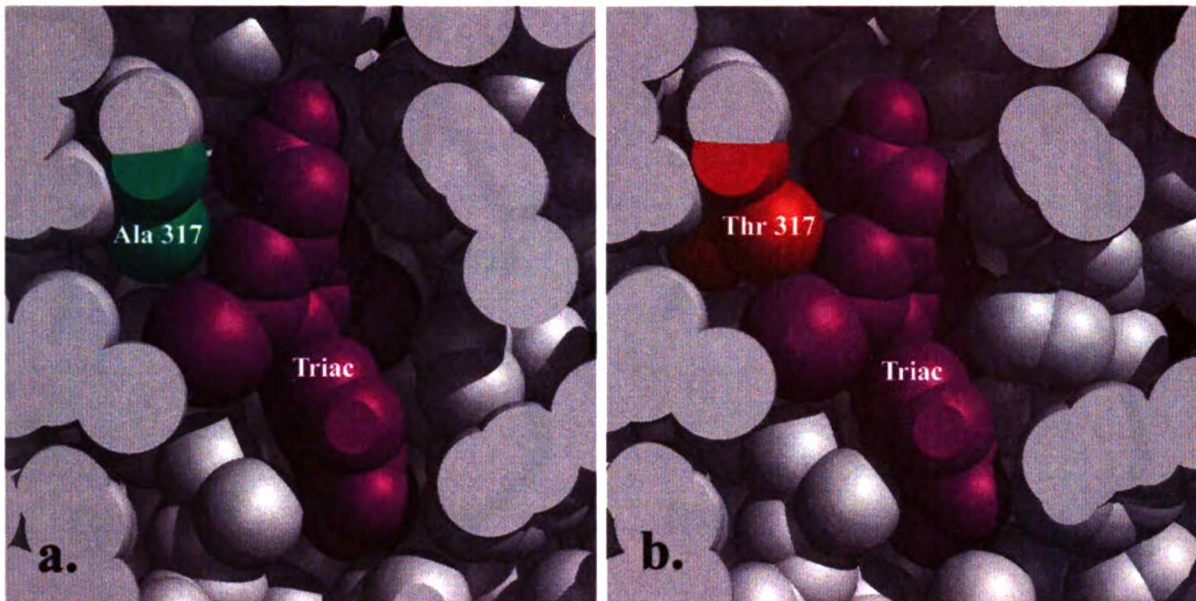
**Figure 1-2: Comparison of the A317T ligand-binding pocket with that of the native receptor.**

In this schematic a slice of the ligand binding pocket in sphere representation has been used to illustrate the structural shift that occurs in the mutant structure. The ligand in both structures is the synthetic hormone Triac, which is colored purple. The site of mutation changes from green in the native structure to dark orange in the A317T mutant. The remainder of the receptor is colored gray.
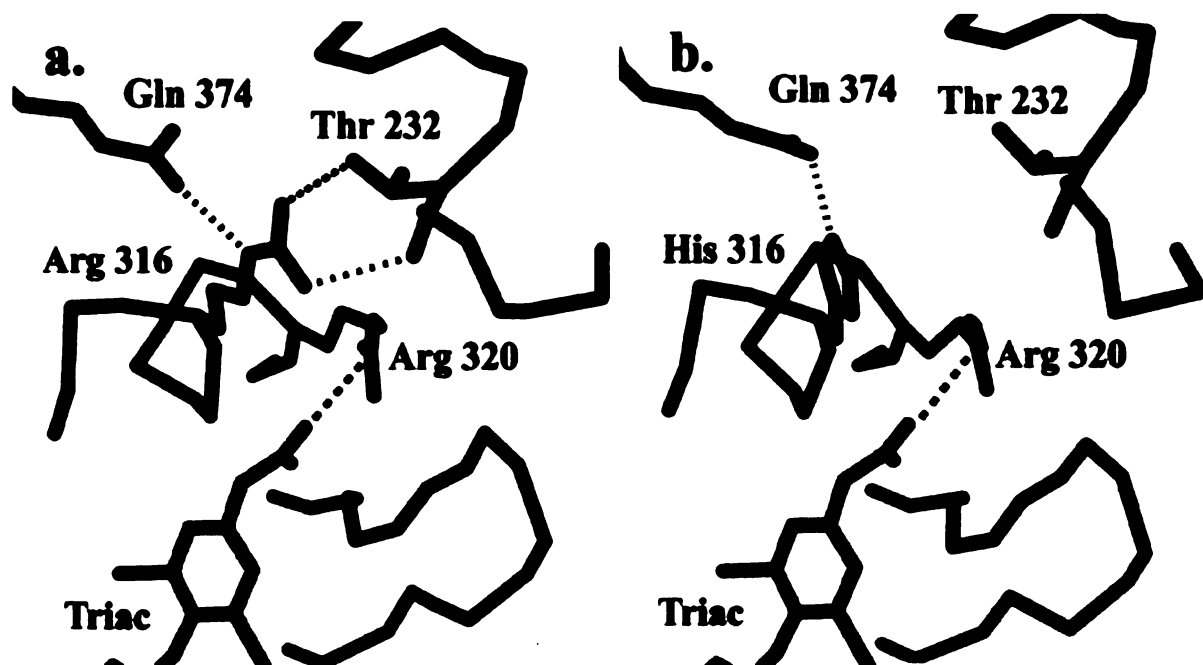
**Figure 1-3: Comparison of the R316 ligand-binding pocket with the native structure.**

Structural elements of the polar region of the hormone-binding pocket are displayed in stick representation. Carbon atoms are either green for the receptor or gray for the ligand. Nitrogen, oxygen and Iodine are blue, red and purple respectively. a. Polar pocket of the native hTRβ. Arg 316 makes three side chain hydrogen bonds with the receptor. One of these bonds is with Gln 374 (part of helix 9). The other two hydrogen bonds are with residue Thr 232 in helix 1. b. Polar pocket of the R316H mutant. The mutation to His 316 preserves the hydrogen bond with Gln 374, but eliminates both of the hydrogen bonds with Thr 232.
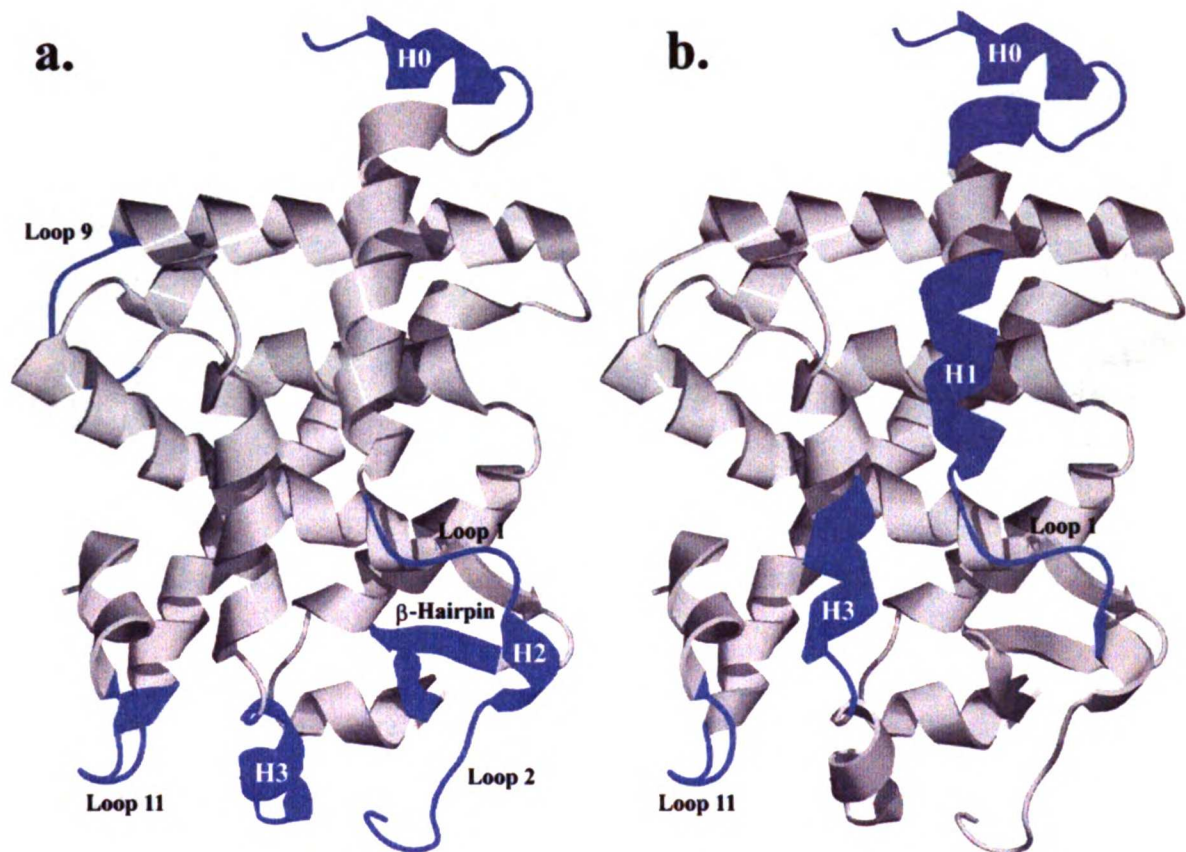
**Figure 1-4: Regions that shift in the mutants A317T and R316H.**

Both mutant structures are schematically displayed in ribbon representation. Regions of the receptors that exhibit a significant RMS shift are colored blue (see methods). The remainders of the receptors are colored gray. a. A317T shows shifts in residues 202-215, 237-274, 327-335, 383-389 and 442-452. These regions correspond to the structural elements helix 0, loop 1 to helix 3, β-hairpin, loop 9 and loop 11. R316H shows shifts in residues 202-221, 227-243, 275-282 and 244-252. These regions correspond to the structural elements helix 0, helix 1, helix 3 and loop 11.
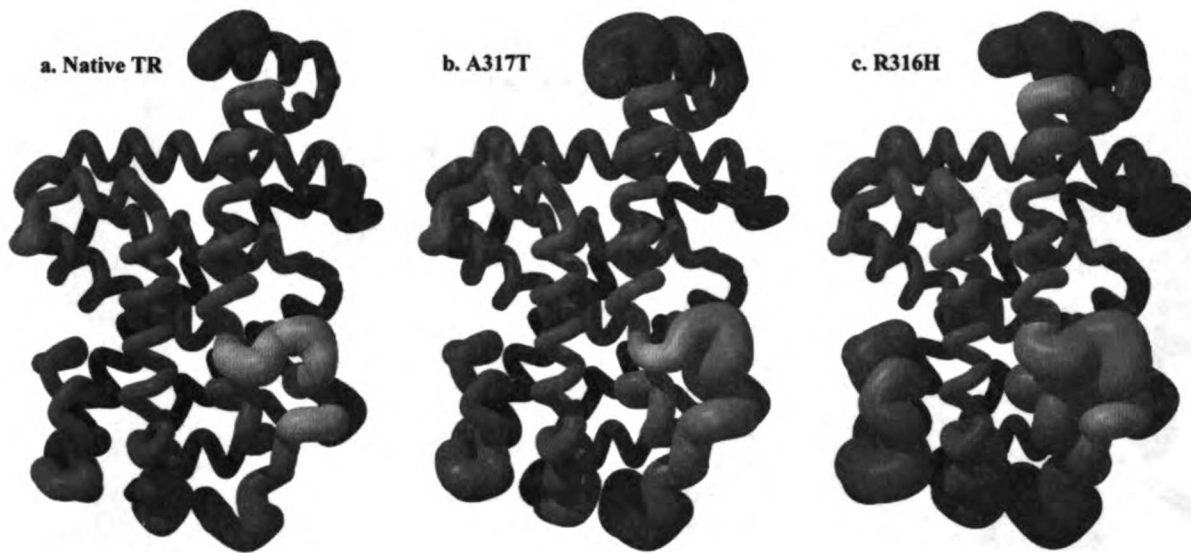
**Figure 1-5: Comparison of normalized thermal B-factors between native, A317T and R316H.**

The b-factor range is represented by both coil radius and color change. The mean value and below is colored green and 1 Å in radius. The top of the range is colored red and 3 Å in radius. a. Normalized B-factors of the native hTRβ model. The regions of the receptor that displayed the highest B-factors are helix 0, the loop following helix 1 and continuing into helix 3 and the helix 11-helix 12 loop. b. Normalized B-factors of the R316H mutant. The regions of the receptor that displayed the highest B-factors are helix 0, the loop following helix 1 and continuing into helix 3, the β-hairpin loop and the helix 11-helix 12 loop. c. Normalized B-factors of the R316H mutant. The regions of the receptor that displayed the highest B-factors are helix 0, the loop following helix 0 and continuing into helix 3 and the helix 11-helix 12 loop.
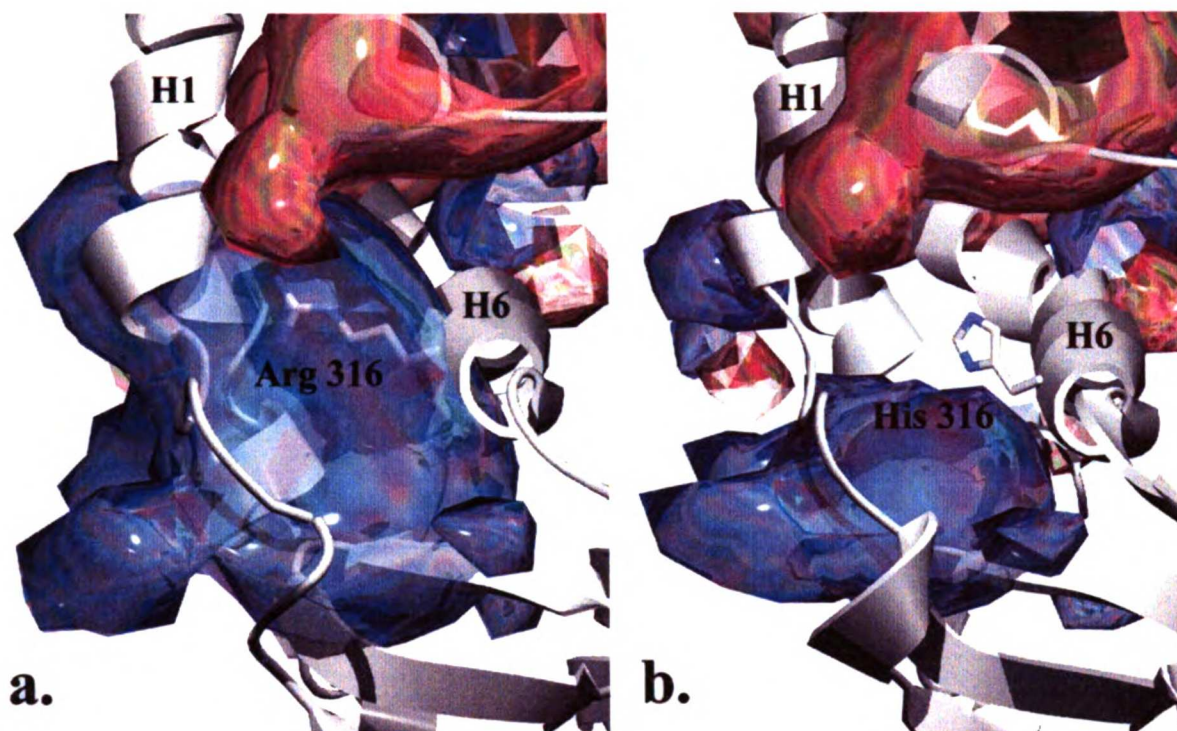
**Figure 1-6: Electrostatic alteration of the polar pocket caused by the R316H mutation.**

These electrostatic potential depictions have been contoured at −5.0 kT/R (red) and +5.0 kT/R (blue.) Carbon and nitrogen are colored gray and blue respectively. a. Electrostatic potential of the native receptor around the Arg 316. The Arg 316 residue is positioned in the center of a large region of positive electrostatic potential. This region is sandwiched between two regions of negative electrostatic potential   b. Electrostatic potential of the mutant around the residue His 316. The mutation to His in R316H eliminates a significant portion of the positive electrostatic potential surrounding residue 316. It appears the mutation cuts the large region of positive electrostatic potential in the native structure into two much smaller regions of positive electrostatic potential.
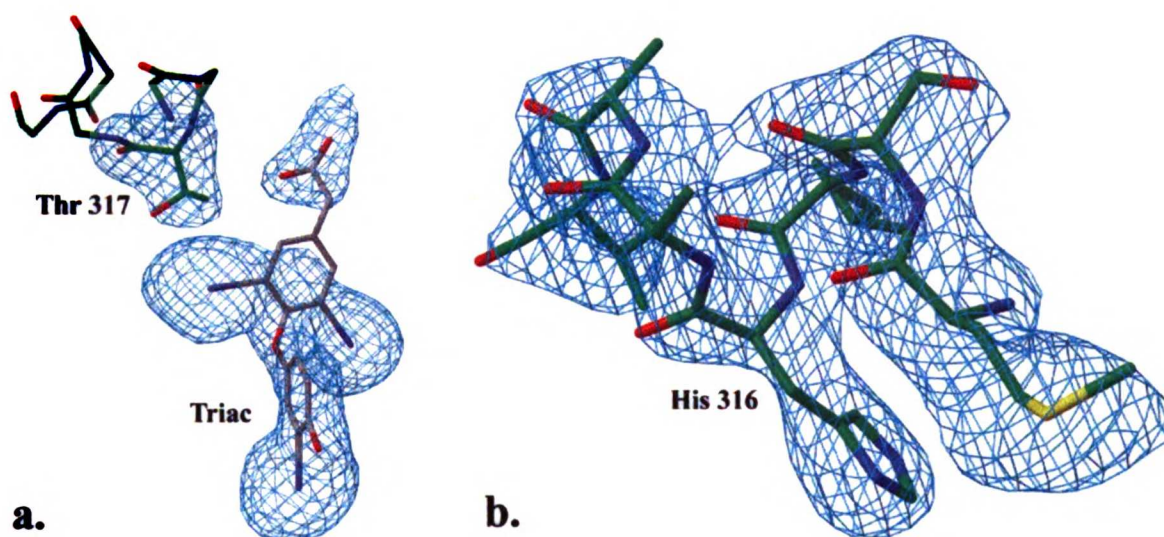
**Figure 1-7: Omit maps of the mutant receptors.**

Omit maps of both mutant receptors were made, omitting the site of mutation and the two neighboring residues. In the A317T omit map, the ligand was also omitted due to the close proximity of the mutation to the ligand. Both figures were colored using the same color scheme. Carbon, oxygen, nitrogen and iodine were colored green, red, blue and purple respectively. The blue mesh represents the omit map contoured at 2 sigma. a. Omit map of R316H. The omit map clearly shows the position of the mutated His residue. b. Omit map of A317T. The map shows the position of both the mutated side chain as well as the ligand. Density for the Thr side chain clearly indicates one rotimer conformation.

47

# References

1.  Carlson-Jurica M, Schrader W, O'Malley B 1990 Steroid receptor family: structure and function. 11:201-220

2.  Lazar MA 1993 Thyroid hormone receptors: multiple forms, multiple possibilities. 14:184-193

3.  Mangelsdorf DJ, Thummel C, Beato M, Herrlich P, Schütz G, Umesono K, Blumberg B, Kastner P, Mark M, Chambon P, et al. 1995 The nuclear receptor superfamily: the second decade. Cell 83:835-9

4.  Beato M, Herrlich P, Schutz G 1995 Steroid hormone receptors: many actors in search of a plot. 83:851-858

5.  Kastner P, Mark M, Chambon P 1995 Nonsteroidal nuclear receptors: what are genetics telling us about their role in real life. 83:859-870

6.  Evans RM 1988 The steroid and thyroid hormone receptor superfamily. Science 240:889-95

7.  Mangelsdorf D, Evans RM 1995 The RXR heterodimers and orphan receptors. 83:841-850

8.  Pinsky L, Trifiro MA, Kaufman M, al. e 1992 Androgen resistance due to mutation of the androgen receptor. J. Clin. Invest. 90:2097-2101

9.  Hurley DM, Accili D, Stratakis CA 1991 Point mutation causing a single amino acid substitution in the hormone binding domain of the glucocorticoid rceptor in familial glucocorticoid receptor in familial glucocorticoid resistance. 87:680-686

10. Komesaroff PA, Funder JW, Fuller PJ 1994 Hormone-nuclear receptor interactions in health and disease. Mineralocorticoid resistance. Bailliere's Clin. Endocrinol. Metab. 8:333-355

11. Rut AR, Hewison M, Kristjansson K, Luisi B, Hughes MR, O'Riordan JL 1994 Two mutations causing vitamin D resistant rickets: modelling on the basis of steroid hormone receptor DNA-binding domain crystal structures. Clin Endocrinol (Oxf) 41:581-90

12. Refetoff S, Weiss R, Usala S 1993 The Syndromes of Resistance to Thyroid Hormone. 14:348-398

13. Collingwood TN, Wagner R, Matthews CH, Clifton-Bligh RJ, Gurnell M, Rajanayagam O, Agostini M, Fletterick RJ, Beck-Peccoz P, Reinhardt W, Binder G, Ranke MB, Hermus A, Hesch RD, Lazarus J, Newrick P, Parfitt V, Raggatt P, de Zegher F, Chatterjee VK 1998 A role for helix 3 of the TRbeta ligand-binding domain in coactivator recruitment identified by characterization of a third cluster of mutations in resistance to thyroid hormone. EMBO J 17:4760-70

14. Safer JD, Cohen RN, Hollenberg AN, Wondisford FE 1998 Defective release of corepressor by hinge mutants of the thyroid hormone receptor found in patients with resistance to thyroid hormone. J Biol Chem 273:30175-82

15. Wagner RL, Apriletti JW, McGrath ME, West BL, Baxter JD, Fletterick RJ 1995 A structural role for hormone in the thyroid hormone receptor. Nature 378:690-7

16. Wagner R, Huber B, Shiau A, Kelly A, Cunha-lima ST, Scanlan T, Apriletti J, Baxter JD, West BL, Fletterick RJ 2001 Hormone Selectivity in Thyroid Hormone Receptors. 15:398-410

17. Adams M, Matthews C, Collingwood TN, Tone Y, Beck-Peccoz P, Chatterjee KK 1994 Genetic analysis of 29 kindreds with generalized and pituitary resistance to thyroid hormone. Identification of thirteen novel mutations in the thyroid hormone receptor beta gene. J Clin Invest 94:506-15

18. Parrilla R, Mixson AJ, McPherson JA, McClaskey JH, Weintraub BD 1991 Characterization of seven novel mutations of the c-erbA beta gene in unrelated kindreds with generalized thyroid hormone resistance. Evidence for two "hot spot" regions of the ligand binding domain. J Clin Invest 88:2123-30

19. Behr M, Loos U 1992 A point mutation (Ala229 to Thr) in the hinge domain of the c-erbA beta thyroid hormone receptor gene in a family with generalized thyroid hormone resistance. Mol Endocrinol 6:1119-26

20. Onigata K, Yagi H, Sakuri A, al. e 1995 A novel point mutation (R243Q) in exon 7 of the c-erbA b thyroid hormone receptor gene in a family with resistance to thyroid hormone. 5:355-358

21. Ribeiro RC, Apriletti JW, Wagner RL, West BL, Feng W, Huber R, Kushner PJ, Nilsson S, Scanlan T, Fletterick RJ, Schaufele F, Baxter JD 1998 Mechanisms of thyroid hormone action: insights from X-ray crystallographic and functional studies. Recent Prog Horm Res 53:351-92; discussion 392-4

22. Geffner ME, Su F, Ross NS, Hershman JM, Van Dop C, Menke JB, Hao E, Stanzak RK, Eaton T, Samuels HH, et al. 1993 An arginine to histidine mutation in codon 311 of the C-erbA beta gene results in a mutant thyroid hormone receptor that does not mediate a dominant negative phenotype. J Clin Invest 91:538-46

23. Takeda K, Weiss RE, Refetoff S 1992 Rapid localization of mutations in the thyroid hormone receptor-beta gene by denaturing gradient gel electrophoresis in 18 families with thyroid hormone resistance [see comments]. J Clin Endocrinol Metab 74:712-9

24. Hayashi Y, Weiss RE, Sarne DH, Yen PM, Sunthornthepvarakul T, Marcocci C, Chin WW, Refetoff S 1995 Do clinical manifestations of resistance to thyroid hormone correlate with the functional alteration of the corresponding mutant thyroid hormone-beta receptors? J Clin Endocrinol Metab 80:3246-56

25. Collingwood TN, Adams M, Tone Y, Chatterjee VK 1994 Spectrum of transcriptional, dimerization, and dominant negative properties of twenty different mutant thyroid hormone beta-receptors in thyroid hormone resistance syndrome. Mol Endocrinol 8:1262-77

26. Forman BM, Yang CR, Au M, Casanova J, Ghysdael J, Samuels HH 1989 A domain containing leucine-zipper-like motifs mediate novel in vivo interactions between the thyroid hormone and retinoic acid receptors. Mol Endocrinol 3:1610-26

27. Pissios P, Tzameli I, Kushner PJ, Moore DD 2000 Dynamic Stabilization of Nuclear Receptor Ligand Binding Domains by Hormone or Corepressor Binding. 6:245-253

28. Johnson BA, Wilson EM, Li Y, Moller DE, Smith RG, Zhou G 2000 Ligand-Induced Stabilization of PPARγ Monitoured by NMR Spectroscopy: Implications for Nuclear Receptor Activation. 298:187-194

29. Apriletti JW, Baxter JD, Lau KH, West BL 1995 Expression of the rat alpha 1 thyroid hormone receptor ligand binding domain in Escherichia coli and the use of a ligand-induced conformation change as a method for its purification to homogeneity. Protein Expr Purif 6:363-70

30. Otwinowski Z, Minor W 1997 Processing of x-ray diffraction data collected in oscillation mode. 276:307-326

31. Brunger AT, Adams PD, Clore GM, DeLano WL, Gros P, W. G-KR, Jiang JS, Kuszewski J, Nilges M, S. PN, Read RJ, Rice LM, Simonson T, Warren GL 1998 Crystallography and NMR system: a new software suite for macromolecular structural determination. Acta Crystallogr D 24:905-921

32. 4 CCPN 1994 The CCP4 suite: programs for protein crystallography. Acta Crystallogr D 50:760-763

33. Kissinger CR, Gehlhaar DK, Fogel DB 1999 Rapid automated molecular replacement by evolutionary search. Acta Crystallogr D Biol Crystallogr 55:484-91

# Chapter 2: Third Cluster Mutations of the Thyroid Hormone Receptor Affect Stability and Position of Loop One

## Introduction

Hormone resistance in the thyroid hormone receptor is often a result of point mutations within the receptor. These mutations cause a syndrome know as resistance to thyroid hormone and generally leads to an excess of thyroid hormone with a generally euthyroid state of the affected individual (1). For many of the RTH mutants there is a correlation between the concentration of free hormone in a patient with the syndrome and the affinity of the mutant receptor (2). However, specific RTH point mutants have been identified that produce the syndrome without significantly decreasing the affinity of the TR for the hormone.

The TR is a member of the nuclear hormone receptor family. The nuclear hormone receptor family encompasses the steroid hormone receptors, retinoic acid receptor (RXR), vitamin D receptor, peroxizome proliferation activator receptor (PPAR), as well as many orphan receptors for which no hormones have yet been found (3-8). These receptors act as monomers, homodimers, heterodimers and heterotetramers on DNA response elements to initiate transcription.

The TR is organized into three domains. The amino-terminal domain is referred to as the A/B domain, which is a context dependent transcriptional activator other nuclear receptors (9, 10). The second domain is the DNA binding domain or C domain. This region is made up of two characteristic zinc finger motifs (11), which recognize and bind to cognate DNA binding sites. The third domain is the LBD or E domain, which encapsulates the thyroid hormone (12). Additionally, this region binds coactivators, corepressors and contains a region partially responsible for the formation of dimers. This domain transmits the binding

state of the receptor and allows other interacting proteins to recognize when hormone has bound to the receptor. The hinge region connects the LBD and DBD. This region is involved in the interaction with corepressor (13, 14).

TR forms complexes with corepressors and a host of other proteins in the unliganded state. Corepressors such as SMRT, NCoR and RIP13, contain the consensus sequence LXXII (14, 15), while mutational analysis with TR showed that three surfaces affect binding of corepressor (Marimuthu et al., unpublished results). At least one of these surfaces is presumed to bind the LXXII motif in a context dependent fashion. Binding of hormone to the TR causes the dissociation of corepressor and the recruitment of coactivator. This process involves a shift in the position of the amphipathic helix twelve already seen in the structures of the estrogen receptor (16), RXR (17) and PPAR (18). Once helix 12 is in place it forms a hydrophobic groove, which coactivators such as GRIP1 can interact with through the consensus coactivator sequence LXXLL (19).

Mutations associated with RTH, lie exclusively in the LBD of the TRβ. These mutations fall into three clusters. The first and second clusters correspond to residues 310-353 and 429-461 respectively. The third cluster is a more recently identified region, that contains residues 234-282 (20). Many mutations in the first and second cluster occur in the hormone-binding pocket of TR and alter the affinity of the thyroid hormone through direct contact with the hormone. Others alter the protein stability of the receptor thus increasing the hormone off rate. Some of the RTH mutants are found on the surface of the receptor clustering around the coactivator-binding site (21). These mutations usually have a lesser effect on hormone affinity; rather they prevent coactivator from associating. Still there are many RTH mutations that do not fit into any of these categories. Two such mutants are

A234T and R243Q (22). Both of these mutations are found in the third cluster of mutations (20) and exhibit defective corepressor release with near normal hormone binding (23).

Here we present the structures of A234T and R243Q and a set of assays to assess the structural properties of these mutant receptors. With these studies we show how these mutations change the structure of the receptor and disrupt function. The principals that we relate may be general to the nuclear receptor family with broader significance to other nuclear receptor hormone resistance syndromes.

## Results

### General Fold of the Mutants

Both mutants display the classic nuclear receptor fold a three-layer stack of 12 $\alpha$-helices with a small region of $\beta$-sheet next to the ligand-binding pocket as seen in figure 2-1a. The resulting structures were similar to the native structure (24) with an overall RMSD of 0.77 and 0.48 for A234T and R243Q respectively. The top of the receptor in figure 2-1a is the hydrophobic core of the protein, while the bottom of the receptor is the ligand-binding pocket. Both structures also include helix 0, which links the LBD to the DBD. A234T and R243Q are found early in the third cluster of RTH mutations as seen in figure 2-1b. The A234T mutation is found at the terminus of helix one leading into loop 1, while the R243Q mutant is found in loop 2.

The A234T mutation prematurely terminates helix one and alters the conformation of loop 1. The Thr 234 side chain in the A234T mutant occupies the same hydrophobic indentation on the body of the receptor that Ala 234 occupies in the native structure.

56

However, the larger side chain of Thr 234 pushes loop one away from the body of the receptor. Loop one rearranges to accommodate the mutation. However, this shift results in higher mobility of loop 1.

The R243Q mutation disrupted helix 2. Helix 2 in the native structure is a single $\alpha$-helical turn (residues 239-243). These same residues formed a coil in the R243Q structure that extended away from the receptor and formed a new crystal contact between residues 235-242 and residues 291-286 in the symmetry related molecule. It is likely that this high mobility crystal contact altered the crystal packing forces, thus leading to the increased mosaicity and altered crystal lattice constants that were observed in the R243Q mutant.

## Structural Changes in the A234T and R243Q Mutants

Regions of the two mutants that shifted the least as a result of the mutation were used to align the mutants with the native structure. The regions that shifted least were identified with DDMP (25) that highlights $\alpha$-carbon atoms that differ most in comparing distances within the LBD. Regions that were most similar correspond to residues 213-232, 278-318, 338-380 and 392-443. All comparative analyses were performed using these residues for alignment. The site of A234T mutation is at the terminus of helix 1 leading into loop 1 (figure 2-1a). The most significant structural shift was observed in this region and continuing through helix 2 and into loop 2. Residues 234-237 shift an RMS distance of 3.66Å. A smaller shift is observed in the five-residue loop following helix eleven (residues 445-449), which shifts an RMS distance of 1.28Å. The regions that shift were located at the bottom face of figure 2-1a and are composed of loop one, helix 2 and loop 2. These structural elements and helix 1 define the hinge region of the receptor. Though the hinge

region of the receptor does not make direct contact with the ligand it does cap the polar end of the ligand binding pocket and packs against the b-hairpin, which forms direct contacts with the ligand.

The native structure shows that the methyl side chain of Ala 234 occupies a small hydrophobic patch located at the interface of helix one and the body of the receptor. Mutation of Ala to Thr at this position introduces a larger group into the interface between helix one and the β-hairpin loop. The structure of the mutant receptor shows a shift of residue 234 away from the body of the receptor as well as termination of helix one at the site of mutation. The steric interaction between the Thr 234 side chain and the amide carbonyl group of Thr 234 causes the carbonyl to rotate away from the side chain by 42° as seen in figure 2-2b. The A234T mutation improves the backbone geometry of the mutant; the backbone angles are all in favored regions. In the native structure loop 2 exhibits the poorest backbone geometry, with two residues in a less favorable conformation. The poor fit may derive from weak electron density resulting from multiple conformations of loop two. It appears that the A234T mutation locks in one conformation of loop two, which results in a more realistic backbone geometry for residues 235 and 236. A comparison of the structures for the native and A234T mutant can be seen in figures 2-2a and 2-2b.

The mutation R243Q is found in the loop following helix two. The major shift observed in the structure is found in the loop following helix one, in helix two and in the loop following helix two. These structural elements, which correspond to residues 233-243, shift an RMS distance of 1.69Å. The loop following helix eleven (residues 445-449) also shifts an RMS distance of 1.10Å. These regions are the same ones that are observed to shift in the

58

A243T structure suggesting that these regions are structurally interdependent. A comparison of the native and R243Q mutant structures can be seen in figures 2-2c and 2-2d.

In the native hTRβ structure Arg 243 forms a salt bridge with Asp 322. In the R243Q mutant Gln 243 is unable to form a salt bridge with residue Asp 322 both because of its shorter side chain and the absence of charge. The Gln 243 side chain instead forms a hydrogen bond with the backbone of Lys 242. The loop containing Trp 239 shifts an RMS distance of 2.3 Å away from the native position and forms a crystal contact between Ala 235 and Glu 295 in the symmetry related molecule.

The electron density map of the region containing the mutation A234T, seen in figure 2-3a, clearly shows the position of the mutated residue as well as the surrounding residues. The largest shift observed in the R243Q structure was in the residues following helix one. This area of the receptor with the exception of residues His 238 and Trp 239 was poorly defined in the electron density map. These two clearly defined residues were used as an anchor to refine the remainder of this region. An electron density map of the residues 238 and 239 is shown in figure 2-3b.

## Disorder in the loop segments

The average B-factors in the A243T mutant structure are 6.7 Å$^2$ higher than in the native structure. This is certainly in part the result of the quality of the particular crystal, but may also be a result of higher overall mobility in the A234T structure. Comparison of absolute B-factors is not informative since B-factors may vary from crystal to crystal; rather we have compared simply scaled B-factors to assess relative changes. For this purpose both the native and mutant B-factors were linearly scaled using residues 264-440. These residues

showed the least amount of positional shift and also had a similar overall distribution of B-factors in both mutant structures and the native structure. When mutant and native receptor B-factors are compared it is clear that the region containing the mutation possess higher mobility in the mutant receptor (see figures 2-4a and 2-4b).

The average B-factors observed in the R243Q mutant structure were 96.6 $\text{Å}^2$ This unrealistic measure of disorder is higher than observed for the native TR, 47.9 $\text{Å}^2$, presumably drawing from the lower resolution (2.9 Å vs. 2.7 Å for the native receptor), and higher mosaicity. The R243Q structure like A234T displayed a similar distribution of b-factors and structural similarity to the native receptor in residues 264-440. B-factors were scaled using residues 264-440. The loop following helix one and continuing into helix three showed much higher relative B-factors and the loop following helix eleven showed slightly higher relative B-factors (see figures 2-4a and 2-4c). The distribution of B-factors in loop 2 was almost uniform unlike the wild type structure, which shows a range of B-factors (figures 2-4a and 2-4c). These regions of high relative B-factor in R243Q correspond to the same regions of increased relative B-factor in A234TFor both structures a combination of small structural shifts with high B-factors, suggest mobility rather than conformational rearrangement.

**Ligand binding Assays**

These studies of hormone binding affinity were performed with hTR E202-461 construct rather than a full-length TR constructs and so differs from earlier reports. Previous studies have determined that the hormone binding affinity of A234T and R243Q mutant TR's as being 50% and 100% of the native receptor, when using $T_3$ as the ligand. Our values for

T₃ association to hTRβ LBD were weaker by an order of magnitude (~10% of native) for both mutant receptors: see table 2. Since the interaction between the LBD and DBD is absent in our assay we are only observing the affect of mutation in the LBD context.

## Assembly assay

A fragment of the hTRβ containing residues 204-260 can bind to a truncated hTRβ containing residues 261-461 in the presence of hormone or corepressor (26). The fragment containing residues 204-260 referred to as the hinge region contains part of helices 0 and 1 and continues through loop 2. This assay was used to determine how mutations in the hinge region would affect the assembly of the TR in the presence of hormone. The A234T and R243Q mutations were introduced into the hinge fragment described above and assembly with hTRβ 261-461 in the presence of increasing concentrations of hormone. Both A234T and R243Q hinge fragments displayed impaired assembly as measured through a luciferase reporter assay when compared to a native hTRβ control. Even at superphysiological concentrations of hormone these mutations prevented full assembly of the receptor with the hinge fragment. The A234T mutant displayed the most severe impairment of assembly and showed only half the luciferase signal of the native receptor at the highest hormone concentration. This observation is consistent with the observation that the transcriptional impairment of this mutant cannot be reversed with high concentrations of hormone (20). The R243Q mutant was less impaired in the assembly assay than A234T; at the highest hormone concentration the signal was ~90% of the native receptor. Curiously R243Q also possessed a very high luciferase signal, almost twice that of the native receptor, in the absence of hormone. The increased activation R243Q in the luciferase reporter system in the absence of

61

hormone may simply be an artifact of the assembly assay, perhaps resulting from more favorable electrostatic interactions between the hinge fragment and the unliganded receptor. However, this might also suggest that the flexible hinge fragment of R243Q can more easily interact with unliganded receptor than the less flexible native hinge region. The results of the assembly assay are summarized in table 2.

## Discussion

### Hinge mutants interaction with hormone

In vitro, the LBD construct of A234T displayed twenty fold less apparent hormone affinity than the native LBD. In previous in vitro studies, the A234T mutation binds hormone with three fold less affinity than the native hTRβ full-length receptor (27). Thus, the A234T mutant shows a six-fold decrease in hormone affinity when assayed as the smaller LBD construct rather than the full-length hTRβ. A similar effect is observed in the R243Q mutant. The LBD construct of R243Q in vitro showed an affinity eighty-fold lower than native hTRβ LBD. Conversely, the full length R243Q mutant in vitro displays native hormone affinity (28). This amounts to a hundred-fold decrease in hormone affinity for R243Q between full length TR and the LBD construct. Observing the ratio of hormone association between LBD and full length receptor it is clear that the R243Q destabilizes the shorter LBD construct. Interestingly, both mutant constructs displayed significantly decreased hormone affinity in the LBD construct, but near native hormone affinity in the full-length construct. Both of these mutations in the LBD context had a significant impact on hormone binding. The decrease in hormone association was of the same order as that observed in mutations that directly interfere with ligand contacts such as A317T and R316H.

It is interesting to note that a mutation in the hinge region could have the same impact on ligand affinity as one found in the pocket, but the full-length receptor masks the effect. The affinity data and the crystallographic data showing disorder in the DBD to LBD linkage suggests that mutations of the hinge region may have a significant impact on LBD stability, which manifests as delayed corepressor release and defective heterodimer formation in the full-length receptor.

The A234T mutation disrupts helix one interaction with the body of the receptor. The A234T mutation added a larger side chain into the interface between helix one and the body of the receptor. In the native structure Ala 234 fits into a small hydrophobic patch formed by helix three, helix six and the β-hairpin. The A234T mutation introduced a larger side chain into this interface, shifting both Thr 234 and loop 1 away from the receptor body. The Thr 234 side chain still occupies the same pocket observed for Ala 234. Oddly, the geometry of the backbone was locked into an apparently more favorable conformation in the adjacent residues (235-236) most likely from the elimination of other conformations in this highly flexible region of the receptor. One of the possible outcomes of altering backbone geometry is conformational strain. However, the B-factors in this region of the receptor were slightly higher that the native B-factors. Strain would be expected to decrease mobility rather than increase it. Thus, strain is probably not the cause of defective assembly. Our model of A234T displayed a premature truncation of helix one and a less than optimal fit of the Thr 234 side chain, suggesting that the interaction between helix 1 and the body of the receptor would be compromised. The assembly assay confirmed this suggestion. Even at superphysiological concentrations of ligand, the A234T mutant failed to induce the luciferase reporter assembly assay beyond ~50% of the native TR control.

## The R243Q Mutation increases mobility in the loop following helix one

Even though the experimental B-factors are not reliable for this structure, the relative distribution of these variables suggest that the substitution R243Q allowed the loop following helix one to assume a new conformation and unfold helix two in the process. Clearly the region affected by the mutation, residues 244-270, was far more mobile in the mutant structure than in the native structure. In the native structure of hTRβ Arg 243 forms a salt bridge with Asp 322. The mutant, Gln 243 in hTRβ is not capable of forming this salt bridge and the side chain is too short to form a hydrogen bond with Asp 322. The Gln 243 side chain instead forms a hydrogen bond with the backbone of Lys 242. However, to accommodate this new arrangement the loop following helix one must shift from the native position. This adjustment causes the amide carbonyl of Ala 235 to form a 3.2 Å crystal contact with the carboxylate side chain of Glu 295. The disrupted salt bridge and new crystal contact in the R243Q mutant result in a conformation shift of residues 235-242, which form a mobile coil that extends into a crystal solvent channel. These residues appear to form a weak crystal contact with residues 291-296 in the symmetry related molecule. Equilibrium between this new conformation and the native conformation may be responsible for the high mosaicity observed in the R243Q structure.

Our experiments on the LBD demonstrate how destabilizing the R243Q mutation is on the hinge region of the receptor. This mutation seriously impairs hormone association and has a dramatic affect on mobility in the LBD context, yet doesn't interfere with assembly, suggesting that all of the destabilization takes place in the loop following helix one. Almost certainly this loop does not make direct contact with the NCoR corepressor (Marimuthu et al., unpublished results). We propose that the effect measured as stabilization of corepressor

interactions with the receptor are due to an increased off rate for the hormone that is most likely due to the loss of the salt bridge between the Arg 243 and Asp 322. Loop 1, helix 2 and loop two cap the ligand-binding pocket and cover the $\beta$-hairpin, see figure 2-6. In both mutant structures loop 1, helix 2 and loop 2 are mobile, which may allow the hinge to move away from the native position and uncap the ligand-binding pocket, allowing the ligand to escape. Thus leading to increased ligand $k_{off}$.

**Role of hinge function**

From a structural standpoint helix one is the least mobile element of the hinge fragment exhibiting the lowest B-factors. It forms the majority of the stabilizing interactions between the hinge fragment and the body of the receptor. The interface between helix one and the body of the receptor is disrupted for A234T and assembly of helix 1 is compromised as measured by the weaker luciferase signal. Conversely, the R243Q mutation is found outside of helix one and has lesser effect on assembly. This suggests that mutations interfering with the interaction between helix one and the body of the receptor compromise the linkage to the DBD and possibly dimers and that the binding of the hinge fragment to the body of the receptor is dependant on helix one. Previous studies with the assembly assay have indicated that the hinge fragment will not bind to the body of the receptor in the absence of ligand. This supports a model where hormone associating with the receptor causes a conformational shift in the body of the thyroid hormone receptor, which can then interact with helix one (26). This type of a model is also consistent with the differences observed between the liganded and unliganded PPAR NMR structures (29). In these structures helix one is mostly unstructured in the absence of ligand and becomes structured when ligand is present in the hormone-binding pocket. The hinge region of the receptor has also been

implicated in the ligand induced conformational shift from homodimer to heterodimer. Clearly, the structures of R234T and R243Q show significant alteration in the stability and flexibility of the hinge region, specifically the loop following helix one. The decreased stability is particularly evident in R243Q, where the loop following helix one completely unfolds and becomes highly mobile. Studies of the switch from homodimer to heterodimer in the presence of hormone confirm that hinge mutations disrupt the formation of heterodimer (23). These observations would suggest a correlation between loop one mobility and defective heterodimer formation.

## Corepressor surface and cluster three mutations

Studies of the interaction between the TRβ and corepressor indicate that there are residues, buried under helix one in the liganded structure, which are involved in corepressor interaction (30). Mutational mapping studies of hTRβ indicate that there are three surfaces that can affect binding of the receptor LBD with corepressor (Marimuthu et al., unpublished results). One of these surfaces, the most critical in assays of association, is found under helix twelve and next to helix three. Part of this surface is inaccessible in the liganded structure. Two other surfaces are found adjacent helix one and helix 10 which participates in dimer formation. Mutation of every surface residue of helix one has no effect on corepressor binding, but residues important for stabilizing helix on the body of the receptor, such as Trp 219 strongly affect the binding of corepressor. These data point not to direct interactions with repressor and helix one, but a role for this region in controlling the association equilibria of corepressor receptor and hormone. As stated before helix one binds poorly to the unliganded conformation of the receptor (26). Our data indicate that helix one plays a significant role in the binding of the hinge fragment to the body of the receptor, but not until

the body of the receptor had undergone a conformational shift induced by the presence of ligand. However, the transition to liganded receptor appears to be decoupled from corepressor dissociation in R243Q and A234T. From the structures of these mutants it appears that the loop following helix one is compromised. The higher B-factors in loop one are indicative of flexibility. This suggests that the loop following helix one is still able to complement the binding of corepressor in the presence of ligand. Thus, the shift in the body of the receptor resulting from hormone association becomes decoupled from the dissociation of corepressor

## Materials and Methods

### Vectors

Mutant hTRβ LBD extending from residue E202 to the C-terminal residue D461 was expressed in E. Coli as a His-tagged fusion protein using the vector, pET28a (Novagen). This vector was created by removing the PstI-BamHI fragments of the pET28 TR E202 WT vector (24) and replacing with the PstI-BamHI fragments from the mutated TRs derived from pCDNA vectors (gift of S. Refetoff).

### Protein expression

Mutant hTRβ LBD was expressed in E. coli strain BL21DE3 pLysS (Novagen). After growth in 2X concentrated Lennox broth (Sigma) at 22 C to an $OD_{600}=1.5$, 0.5mM isopropyl β-D thiogalactoside (IPTG, sigma) was added and growth continued for 6h. Cells were harvested by centrifugation and pellets were frozen in liquid N2 and stored at −80 C.

## Purification

Thawed pellets from 1 L culture were lysed in For TR LBD, 50 mM sodium-phosphate pH 8.0, 300 mM NaCl, 10% glycerol, 0.1% monothioglycerol, 1 mM PMSF, 1 mM Benzamidine HCl, with 0.2 mg/ml lysozyme (20 min, 0°C). Extracts were sonicated briefly to break DNA, and centrifuged (Ti45, 36000 rpm, 1h, 4°C). Load lysate on Talon resin (Clontech) equilibrated in sodium phosphate buffer, eluted with 0-300 mM imidazole gradient. Isolation of liganded (3,3', 5-triiodo-L-acetic acid (Triac; Sigma)) receptor using TSK-phenyl HPLC (TosoHaas, Philadelphia) was performed as described (31); *yield* was 3 mg/L bacterial culture. For crystallization, hTR β LBD was diluted into 20 mM Hepes pH 8.0, 3 mM DTT and concentrated to 11.5 mg/ml by ultrafiltration (Millipore UFV2BGC10). The N-terminal His-tag was not removed prior to crystallization.

## Ligand-Binding Saturation Assays

The affinities of binding of $[^{125}I]T_3$ to the hTRβ LBD (WT and mutants) were determined using saturation binding assays as described (24).

## Ligand-Binding Kinetic Assays

For the dissociation experiments, 1nM of $[^{125}I]T_3$ was allowed to bind 10 femtomoles of each receptor, at $4^0$C, until they have reached equilibrium (12 hours). At that point, further binding of radioligand to the receptors was blocked by adding unlabeled ligand, in a concentration 100 times higher (100nM). The receptor-bound $[^{125}I]T_3$ was isolated by gravity flow through a 2mL course Sephadex G-25 (Pharmacia Biotech) column, and quantified using a gamma-counter (COBRA, Packard Instruments, Meriden, CT). Binding curves were

fit by nonlinear regression and the $K_{off}$ values were calculated using the one phase exponential decay equation contained in Prism 3.0 program. The association experiments were performed using 2nM of $[^{125}I]T_3$ and 10 femtomoles of receptor, at $4^0C$. After adding the receptor to the ligand, specific binding was measured immediately and at various times thereafter. 100uL was applied to coarse Sephadex G-25 column at each time and the eluate containing the bound receptor was quantified using a gamma-counter. Binding curves were fit by nonlinear regression and value of $K_{ob}$ determined by fitting an exponential association equation to the data. To calculate the association rate constant ($K_{on}$), expressed in units of Molar-1 min-1, this equation was used: $k_{on} = (k_{ob} - k_{off}) / [radioligand]$. The $K_{on}$ obtained experimentally was compared to the expected $K_{on}$, calculated according to the law of mass action equation: $K_d = k_{off} / k_{on}$.

## Crystallization

The hTRβ LBD harboring the A234T mutation was expressed and purified as previously described for the native hTRβ E202-461 poly-histadine tagged construct (reference to Richards paper). Initial crystals of the A234T mutant bound to TRIAC were found using the previously established conditions for the native hTRβ E202-461 construct in complex with Triac (Methods, Reference). Refinement of the crystallization conditions resulted in a well buffer of 700mM Sodium Acetate and 100mM Sodium Cacodylate adjusted to pH 7.6. Micro seeding was not necessary for optimal growth of the A234T mutant. Crystals were flash frozen in liquid nitrogen after gradually increasing the glycerol concentration through a series of soaks. The cryo solvents contained 900mM sodium acetate, 100mM sodium cacodylate pH 7.6 and a range of glycerol concentrations from 5% to 25% in

five equal steps. These crystals diffracted to 2.4Å at the Stanford Synchrotron Radiation Laboratory (SSRL) 7-1 beam line. The hTRβ E202-461 R243Q mutant was expressed and purified as previously described. Refinement of crystallization conditions produced optimal crystals at 700mM Sodium Acetate and 100mM Sodium Cacodylate adjusted to pH 7.6. Optimum crystals were obtained with micro seeding using hTRβ / $T_3$ crystals crushed with the seed bead kit (Hampton). The cryo solvent was the same as the mother liquor with 300mM Sodium Acetate added and a range of glycerol from 5% to 25% in five equal steps. Crystals of the R243Q mutant diffracted to 2.9Å at the SSRL 7-1 beam line.

## Data Collection and Structural Refinement

An $117^0$ data set of A234T was collected using one-degree oscillations. The data set was found to be 99.7% complete to 2.4Å resolution. Crystals of A234T with Triac bound exhibited the same hexagonal bypymidal morphology found in wild type receptor. Crystals were space group P3121 (a=68.82 Å, c=131.07 Å). Reflections were indexed and scaled using DENZO and SCALEPACK (32). A molecular replacement solution was found with Crystallography and NMR System 1.0 (CNS) (33) rotational search using the wild type TR-β /TRIAC structure with ligand and mutant side chain omitted. The structure was refined with CNS using multiple rounds of simulated annealing and manual rebuilding with the Quanta98 software package. Electron density maps and coordinates were manipulated with the Collaborative Crystallography Project Number Four in Protein crystallography package (CCP4)(34). The resulting structure had an Rcryst of 21.8% and an R-free of 25.7%. An 90° data set of R243Q was collected using one-degree oscillations. This data set exhibited the same space group and morphology as the native data set. The crystal constants were slightly

different (a=b=68.84, c=130.53). The data for this mutant was reduced with denzo and scalepack. An initial molecular replacement solution was found with CNS 1.0 using a rotational search of the native hTRβ with ligand and mutation site omitted. The structure was refined using the same method described for A234T. The final structure exhibited very high b-factors. This is consistent with both the high mosaicity of the crystal (~1.0) and the calculated Wilson b-factor of 85.9. The resulting structure was refined to an R factor of 23.9% and a Free R of 28.7%. The statistics from these refinements are listed in table 1.

## Plasmid construction for assembly assay

Fusion constructs of VP16 and Gal4 with deletions of TR were obtained by PCR amplification of the corresponding region and subcloned into pVP16 and pM vectors respectively (Clontech). For the VP16 fusion, amplified Helix2 to 12 fragment was subcloned as EcoR1/Xho1 into EcoRI/SalI pVP16. Gal4 fusion was obtained by subcloning EcoR1/XbaI fragments into pM. Point mutations were generated with the quickchange site-directed mutagenesis kit according to the manufacturer protocol (Stratagene). All vectors were analyzed by restriction digestion and sequencing.

## Cell culture and transfections for assembly assay

HepG2 cells were grown in Dulbecco's Modified Eagle Medium (DMEM) supplemented with 10% bovine serum. For transfections, the cells were plated the day before into 24-well dishes at 50% density in DMEM supplemented with 10% charcoal-stripped serum. Transfections were performed using Fugene (Roche) for 24 hours. Typically 200ng of reporter construct, 100ng of β-galactosidase expression vector for transfection efficiency control, and 50ng of expression vectors were used. After 24 hours of transfection, the cells

were harvested and assayed for luciferase assays (enhanced luciferase assay kit, PharMingen International) and β-galactosidase activity. All experiments were performed at least three times in triplicates.

## Materials and Methods

### Vectors

The native hTRβ LBD construct containing residues $His_6$ E202-D461 was introduced into pET28a as previously described (33). The A317T and R316H mutations were introduced into the hTRβ E202 construct using cassette mutagenesis. The mutant sequences were transferred to the pET 28 TR-E202 vector with the unique PstI and SalI sites. The sequence was verified by automatic DNA sequencing at the University of California Biological Resource Center

### Protein Expression

Mutant hTRβ LBD was expressed in E. coli strain BL21DE3 PlysS (Novagen, Madison, WI)(22 C, 0.5mM isopropylthiogalactoside added at $OD_{600} = 0.6$, induced 5 h). Cells were harvested by centrifugation and pellets were frozen in liquid N2 and stored at – 80C. Ligand binding studies were preformed with protein expressed with the pET 28 vector using the TNT T7 Quick in vitro translation kits (Promega Corp., Madison WI.)

### Purification

The native, A317T and R316H hTRβ E202 proteins were purified as described previously (33). The protocol was altered so that Triac was added to the initial cell lysis

buffer to protect the mutant receptors from rapid degradation. Yields for both mutants were ~3mg/liter of bacterial culture.

## Ligand-Binding Saturation and Kinetic Assays

For the dissociation experiments, 1nM of $[^{125}I]T_3$ was allowed to bind 10 femtomoles of each receptor, at $4^0C$, until reaching equilibrium (12 hours). Further binding of radioligand to the receptors was blocked by adding unlabeled ligand, at a concentration 100 times higher (100nM). The receptor-bound $[^{125}I]T_3$ was isolated consecutively by gravity flow through a 2mL course Sephadex G-25 (Pharmacia Biotech) column, and quantified using a gamma-counter (COBRA, Packard Instruments, Meriden, CT). Binding curves were fit by nonlinear regression and the $K_{off}$ values were calculated using the one phase exponential decay equation contained in Prism 3.0 program. The association experiments were performed using 2nM of $[^{125}I]T_3$ and 10 femtomoles of receptor, at $4^0C$. After adding the receptor to the ligand, specific binding was measured immediately and at regular intervals thereafter. 100uL was applied to coarse Sephadex G-25 column at each time (same way as for dissociation assays), and the eluate containing the bound receptor was quantified using a gamma-counter. Binding curves were fit by nonlinear regression and value of $K_{ob}$ determined by fitting an exponential association equation to the data. To calculate the association rate constant ($K_{on}$), expressed in units of Molar-1 min-1, this equation was used: $k_{on} = (k_{ob} - k_{off}) / [radioligand]$. The $K_{on}$ obtained experimentally was compared to the expected $K_{on}$, calculated according to the law of mass action equation: $K_d = k_{off} / k_{on}$.

## Crystallization

The hTRβ LBD harboring the A234T mutation was expressed and purified as previously described for the native hTRβ E202-461 poly-histadine tagged construct (reference to Richards paper). Initial crystals of the A234T mutant bound to TRIAC were found using the previously established conditions for the native hTRβ E202-461 construct in complex with Triac (Methods, Reference). Refinement of the crystallization conditions resulted in a well buffer of 700mM Sodium Acetate and 100mM Sodium Cacodylate adjusted to pH 7.6. Micro seeding was not necessary for optimal growth of the A234T mutant. Crystals were flash frozen in liquid nitrogen after gradually increasing the glycerol concentration through a series of soaks. The cryo solvents contained 900mM sodium acetate, 100mM sodium cacodylate pH 7.6 and a range of glycerol concentrations from 5% to 25% in five equal steps. These crystals diffracted to 2.4Å at the Stanford Synchrotron Radiation Laboratory (SSRL) 7-1 beam line. The hTRβ E202-461 R243Q mutant was expressed and purified as previously described. Refinement of crystallization conditions produced optimal crystals at 700mM Sodium Acetate and 100mM Sodium Cacodylate adjusted to pH 7.6. Optimum crystals were obtained with micro seeding using hTRβ / $T_3$ crystals crushed with the seed bead kit (Hampton.) The cryo solvent was the same as the mother liquor with 300mM Sodium Acetate added and a range of glycerol from 5% to 25% in five equal steps. Crystals of the R243Q mutant diffracted to 2.9Å at the SSRL 7-1 beam line.

## Data Collection and Structural Refinement

An $117^0$ data set of A234T was collected using one-degree oscillations. The data set was found to be 99.7% complete to 2.4Å resolution. Crystals of A234T with Triac bound

exhibited the same hexagonal bypymidal morphology found in wild type receptor. Crystals were space group P3121 (a=68.82 Å, c=131.07 Å). Reflections were indexed and scaled using DENZO and SCALEPACK (34). A molecular replacement solution was found with Crystallography and NMR System 1.0 (CNS) (35) rotational search using the wild type TR-β /TRIAC structure with ligand and mutant side chain omitted. The structure was refined with CNS using multiple rounds of simulated annealing and manual rebuilding with the Quanta98 software package. Electron density maps and coordinates were manipulated with the Collaborative Crystallography Project Number Four in Protein crystallography package (CCP4)(36). The resulting structure had an Rcryst of 21.8% and an R-free of 25.7%. An 90° data set of R243Q was collected using one-degree oscillations. This data set exhibited the same space group and morphology as the native data set. The crystal constants were slightly different (a=b=68.84, c=130.53). The data for this mutant was reduced with denzo and scalepack. An initial molecular replacement solution was found with CNS 1.0 using a rotational search of the native hTRβ with ligand and mutation site omitted. The structure was refined using the same method described for A234T. The final structure exhibited very high b-factors. This is consistent with both the high mosaicity of the crystal (~1.0) and the calculated Wilson b-factor of 85.9. The resulting structure was refined to an R factor of 23.9% and a Free R of 28.7%. The statistics from these refinements are listed in table 1.

## Plasmid construction for assembly assay

Fusion constructs of VP16 and Gal4 with deletions of TR were obtained by PCR amplification of the corresponding region and subcloned into pVP16 and pM vectors respectively (Clontech). For the VP16 fusion, amplified Helix2 to 12 fragment was subcloned as EcoR1/Xho1 into EcoRI/SalI pVP16. Gal4 fusion was obtained by subcloning

75

EcoR1/XbaI fragments into pM. Point mutations were generated with the quickchange site-directed mutagenesis kit according to the manufacturer protocol (Stratagene). All vectors were analyzed by restriction digestion and sequencing.

**Cell culture and Transfections for Assembly Assay**

HepG2 cells were grown in Dulbecco's Modified Eagle Medium (DMEM) supplemented with 10% bovine serum. For transfections, the cells were plated the day before into 24-well dishes at 50% density in DMEM supplemented with 10% charcoal-stripped serum. Transfections were performed using Fugene (Roche) for 24 hours. Typically 200ng of reporter construct, 100ng of β-galactosidase expression vector for transfection efficiency control, and 50ng of expression vectors were used. After 24 hours of transfection, the cells were harvested and assayed for luciferase assays (using the enhanced luciferase assay kit, PharMingen International) and β-galactosidase activity. All experiments were performed at least three times in triplicates.

## Data collection

| Data set | Resolution (Å) | Reflections measured | unique | Coverage (%) | *$R_{sym}$ |
|---|---|---|---|---|---|
| hTRß A234T | 2.4 | 80196 | 14565 | 99.6 | 0.051 |
| hTRß R243Q | 2.9 | 54104 | 13743 | 93.5 | 0.055 |

## Refinement

| Data set | Resolution Å | Reflections | §R | §$R_{free}$ | Rms bonds | Rms Angles |
|---|---|---|---|---|---|---|
| hTRß A234T | 2.4 Å | 13085 | 21.3 % | 25.5 % | 0.012 | 1.99 |
| hTRß R243q | 2.9 Å | 12346 | 22.6 % | 26.4 % | 0.010 | 1.434 |

**$R_{sym}= \Sigma_h \ \Sigma_i \ | \ I_{h,i} - <I_h> | / \Sigma \ I_h$ for the intensity ($I$) of $i$ observations of reflection $h$.

§R factor $= \Sigma \ | \ F_{obs} - F_{calc} \ | / \ \Sigma | \ F_{obs} \ |$. $R_{free}$ is calculated the same as the R factor, using 10% of the reflections that were set aside for cross validation and not used in refinement.

Table 2-1: Data collection and refinement statistics for A234T and R243Q

| Receptor | $K_d$ (Molar) | $K_{off}$ (min-1) | $K_{on}$ ($M^{-1}.min^{-1}$) |
|---|---|---|---|
| **Wild Type** | $5.9 \times 10^{-11}$ (+- 2.6) | 0.0059 (+- 0.0006) | $3.7 \times 10^8$ (+- 0.58) |
| **A234T** | $3.8 \times 10^{-10}$ (+- 1.9) | 0.024 (+- 0.08) | $2.5 \times 10^8$ (+- 0.4) |
| **A243Q** | $4.1 \times 10^{-10}$ (+- 2.9) | 0.013 (+- 0.03) | $1.7 \times 10^8$ (+- 0.5) |

Table 1-2: Receptor hormone association ($k_{on}$), dissociation ($k_{off}$) and equilibrum constants ($Kq$) for $T_3$
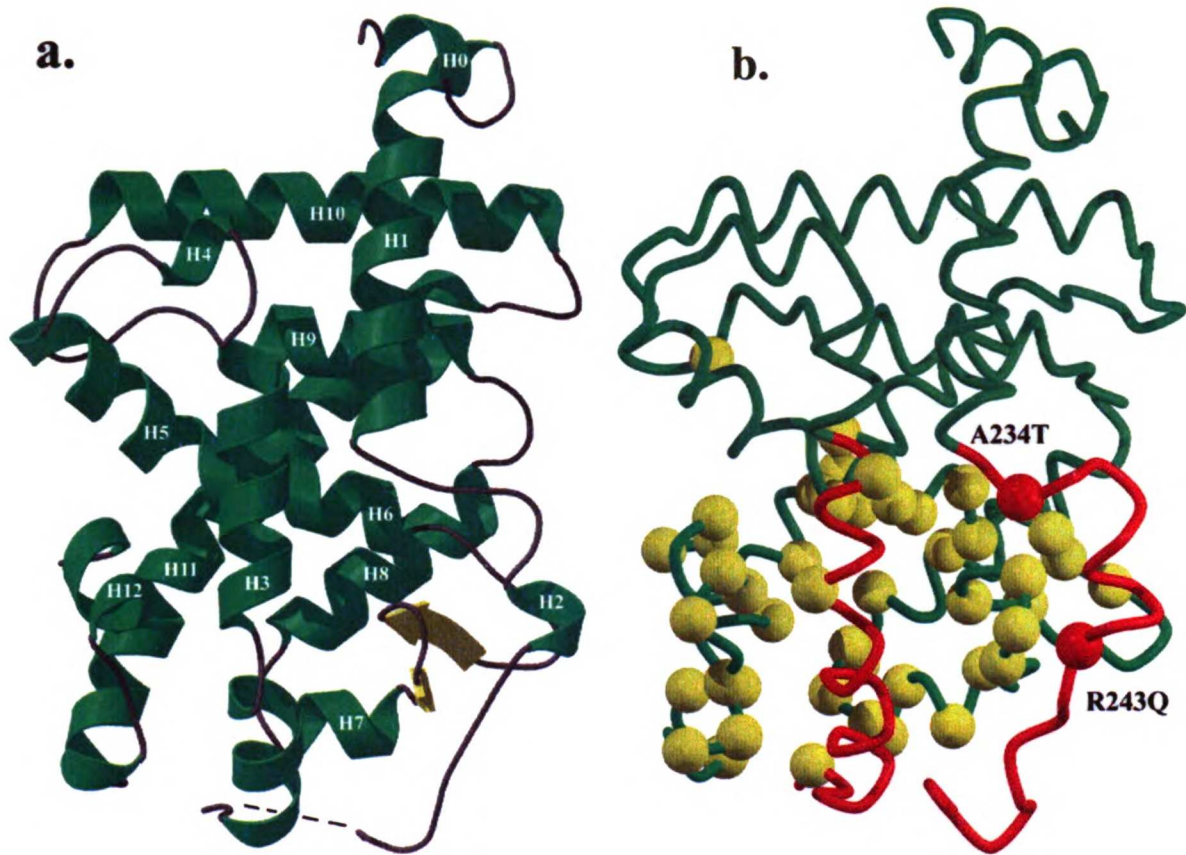
**Figure 2-1: General Fold of the TR and the Locations of the RTH mutants**

a. The twelve α-helices of the TR LBD and helix zero are labeled in this diagram.

The Omega loop has been labeled. The Ligand is represented as purple spheres. Other

regions such as corepressor and coactivator binding sites have been represented as color-

coded transparent surfaces. Blue surfaces correspond to coactivator binding sites, while red

surfaces correspond to corepressor binding sites. b. The sites of RTH point mutants in the

hTRβ. The c-alpha's of the TR are represented as a gray coil. The RTH point mutants are

represented as spheres that are color-coded based on, which group the mutant belongs to.

Group one mutants are colored green, group two mutants are colored blue and group three
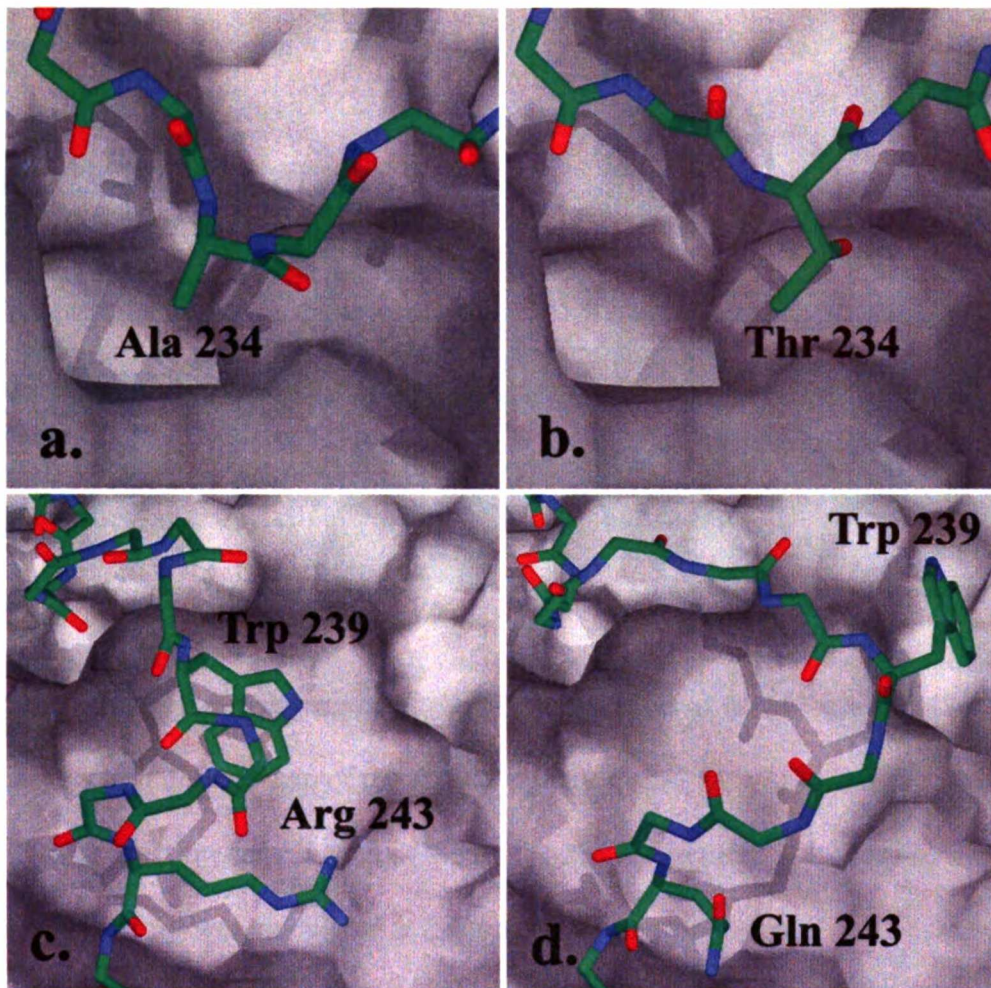
mutants are colored yellow.

**Figure 2-2: Structural shifts observed in A234T ant R243Q Mutants.**

a, Native position of the Ala 234. Stick diagram of helix one terminus and the loop following. Atoms are color-coded green, red and blue to represent carbon, oxygen and nitrogen respectively. The body of the receptor is represented as a molecular surface calculated with a 1.4 angstrom probe. This convention was used for all of figure 2-1. b, Position of the mutant A234T. c, A more inclusive view of the native receptor. This view of the native receptor is used for comparison to the R243Q mutation, which disrupts a significant portion of the loop following helix one. d, Position of the loop following helix one in the R243Q mutant. The loop following helix one swings away from the body of the receptor and forms a new crystal contact.
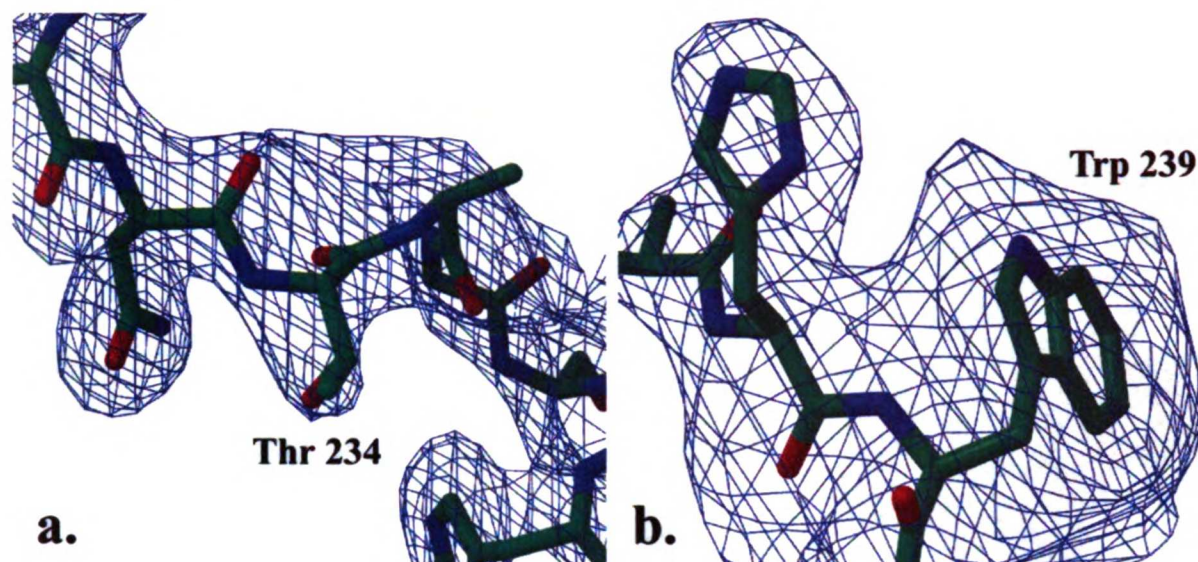
**Figure 2-3: Electron density maps of the Mutation Sites of A234T and R243Q.**

a, Electron density map of the A234T mutation site. Residues 231-237 were omitted from a 1fo-1fc electron density map of the final A234T structure. The blue electron density electron density map was calculated at 2 sigma. Stick representation of atoms are colored by chemical type. Oxygen, red; Nitrogen, blue; Carbon, green. b. Electron density map of the R243Q mutation site. Residues 235-242 were omitted from a 1fo-1fc electron density map of the final R243Q structure to show the position of Trp 239. This figure follows the same conventions as figure 2-3a.
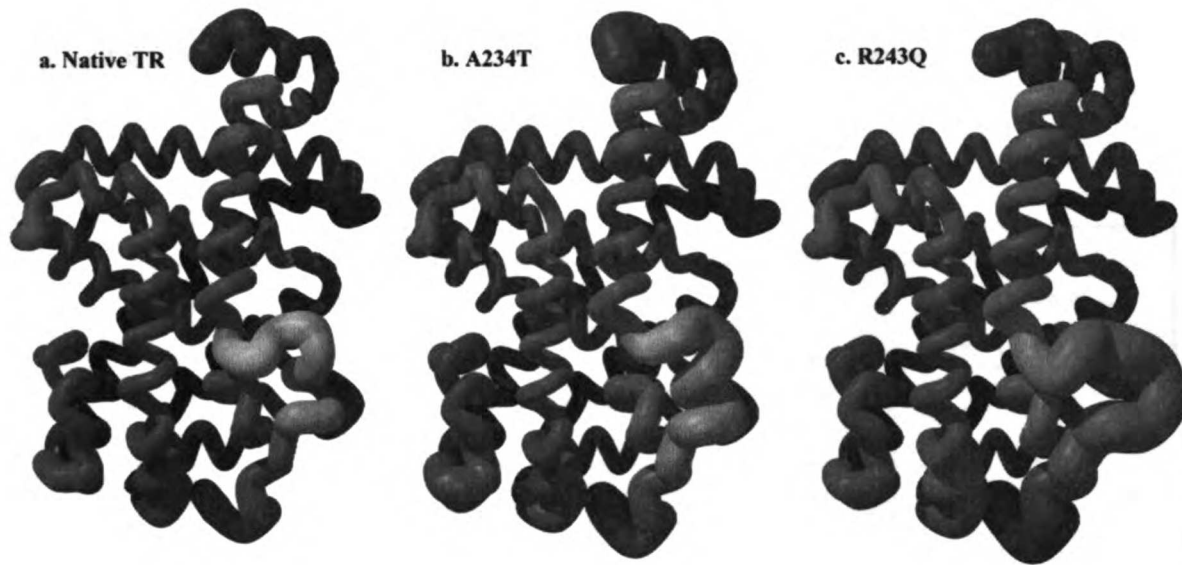
**Figure 2-4: B-factor comparison of Mutants with the Native structure**

Trace thickness and color range represent thermal b-factor range. Sections with lower b-factor are thinner and green, conversely sections with higher b-factor are thicker and red in color. B-factors have been normalized to the range of b-factors observed in residues 270-440 for each individual structure. B-factors color and thickness representation have been scaled in each structure so that the mean temperature or below is green and the highest temperature is red. a, Native hTRβ b-factors. b, A234T b-factors. c, R243Q b-factors.
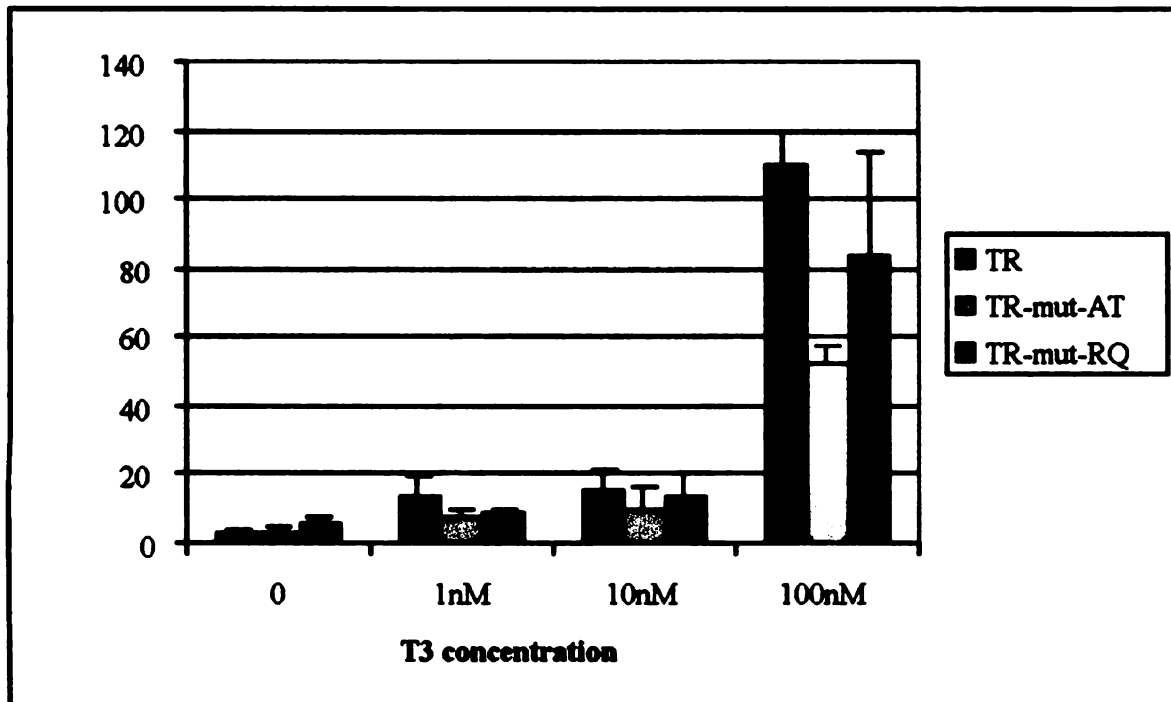
**Figure 2-5: Assembly of the hinge fragment with A234T, R243Q and native hTRβ**

This diagram depicts the luciferase signal produced by the interaction of the hinge

fragment of hTRβ (residues 204-260) with the body of the hTRβ (residues 261-461). The

A234T and R243Q mutations have been introduced into the hinge fragment, while the native

hinge fragment was used as a control. The y-axis represents luciferase signal, while the x-

axis represents the concentration of $T_3$ used for assembly. The signals for native, A234T and

R243Q are blue, yellow and green respectively.

**Figure 2-6: Ligand and b-hairpin exposed by the removal of loop one**

High mobility structural elements of the TRβ Mutants A234T and R243Q have been
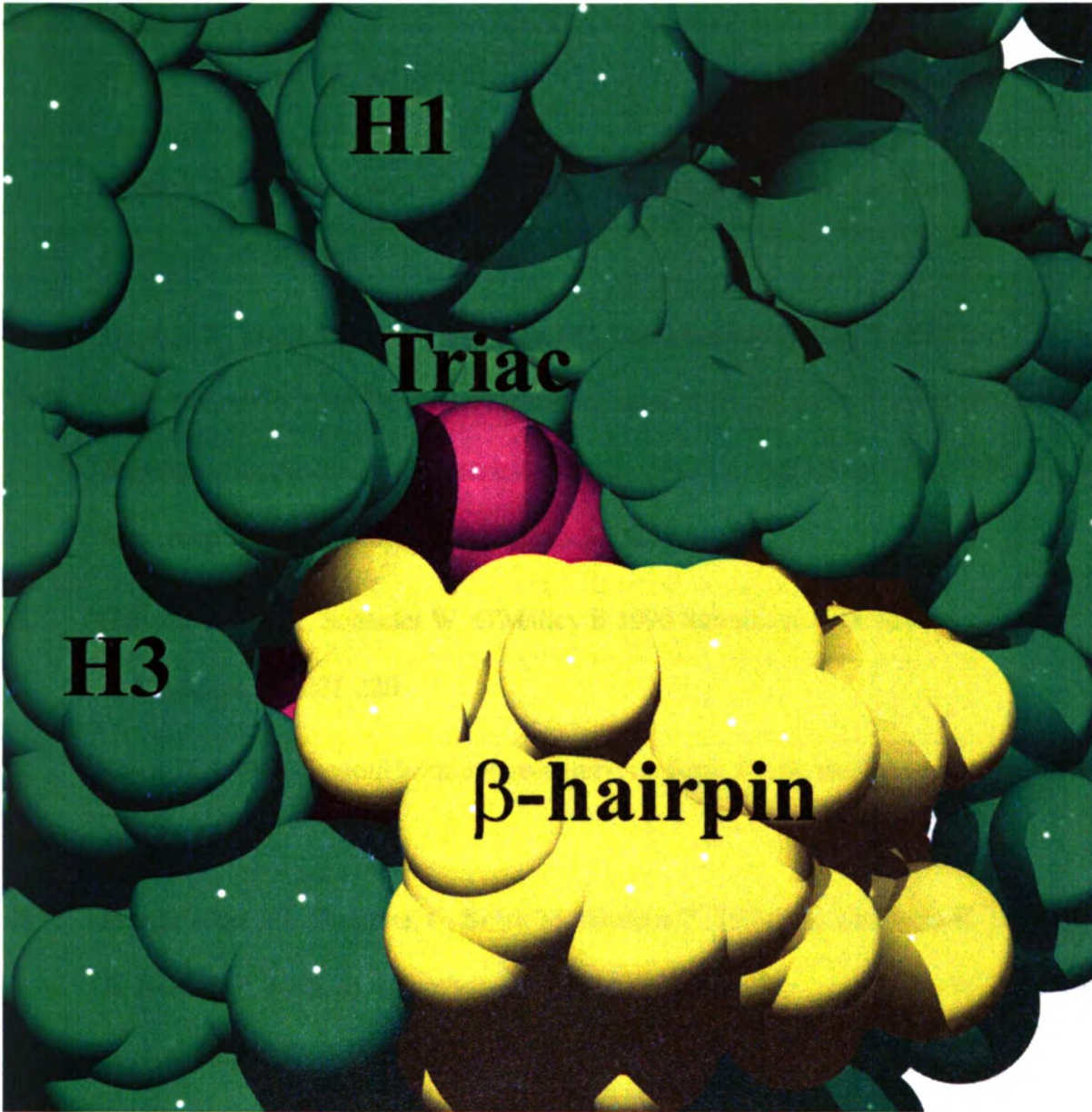removed from this depiction of the receptor. This reveals the β-hairpin and ligand, which are
beneath the hinge region of the receptor. The β-hairpin, ligand and receptor are colored
yellow purple and green respectively.

# References

1. Refetoff S, Weiss R, Usala S 1993 The Syndromes of Resistance to Thyroid Hormone. 14:348-398

2. Hayashi Y, Weiss RE, Sarne DH, Yen PM, Sunthornthepvarakul T, Marcocci C, Chin WW, Refetoff S 1995 Do clinical manifestations of resistance to thyroid hormone correlate with the functional alteration of the corresponding mutant thyroid hormone-beta receptors? J Clin Endocrinol Metab 80:3246-56

3. Carlson-Jurica M, Schrader W, O'Malley B 1990 Steroid receptor family: structure and function. 11:201-220

4. Lazar MA 1993 Thyroid hormone receptors: multiple forms, multiple possibilities. 14:184-193

5. Mangelsdorf DJ, Thummel C, Beato M, Herrlich P, Schütz G, Umesono K, Blumberg B, Kastner P, Mark M, Chambon P, et al. 1995 The nuclear receptor superfamily: the second decade. Cell 83:835-9

6. Mangelsdorf D, Evans RM 1995 The RXR heterodimers and orphan receptors. 83:841-850

7. Beato M, Herrlich P, Schutz G 1995 Steroid hormone receptors: many actors in search of a plot. 83:851-858

8. Kastner P, Mark M, Chambon P 1995 Nonsteroidal nuclear receptors: what are genetics telling us about their role in real life. 83:859-870

9. Langlois MF, Zanger K, Monden T, Safer JD, Hollenberg AN, Wondisford FE 1997 A unique role of the beta-2 thyroid hormone receptor isoform in negative regulation by thyroid hormone. Mapping of a novel amino-terminal domain important for ligand-independent activation. J Biol Chem 272:24927-33

10. Safer JD, Langlois MF, Cohen R, Monden T, John-Hope D, Madura JP, Hollenberg AN, Wondisford FE 1997 Isoform variable action among thyroid hormone receptor mutants provides insight into pituitary resistance to thyroid hormone. 11:16-26

11. Evans RM, Hollenberg SM 1988 Zinc fingers: guilt by association. 52:1-3

12. Wagner RL, Apriletti JW, McGrath ME, West BL, Baxter JD, Fletterick RJ 1995 A structural role for hormone in the thyroid hormone receptor. Nature 378:690-7

13. Baniahmad A, Köhne AC, Renkawitz R 1992 A transferable silencing domain is present in the thyroid hormone receptor, in the v-erbA oncogene product and in the retinoic acid receptor. Embo J 11:1015-23

14. Webb P, Anderson CM, Valentine C, Nguyen P, Marimuthu A, West BL, Baxter JD, Kushner PJ 2000 The nuclear receptor corepressor (N-CoR) contains three isoleucine motifs (I/LXXII) that serve as receptor interaction domains (IDs). Mol Endocrinol 14:1976-85

15. Hu X, Lazar MA 1999 The CoRNR motif controls the recruitment of corepressors by nuclear hormone receptors. Nature 402:93-6

16. Shiau AK, Barstad D, Loria PM, Cheng L, Kushner PJ, Agard DA, Greene GL 1998 The structural basis of estrogen receptor/coactivator recognition and the antagonism of this interaction by tamoxifen. Cell 95:927-37

17. Bourguet W, Ruff M, Chambon P, Gronemeyer H, Moras D 1995 Crystal structure of the ligand-binding domain of the human nuclear receptor RXR-alpha [see comments]. Nature 375:377-82

18. Uppenberg J, Svensson C, Jaki M, Bertilsson G, Jendeberg L, Berkenstam A 1998 Crystal structure of the ligand binding domain of the human nuclear receptor PPARgamma. J Biol Chem 273:31108-12

19. Darimont BD, Wagner RL, Apriletti JW, Stallcup MR, Kushner PJ, Baxter JD, Fletterick RJ, Yamamoto KR 1998 Structure and specificity of nuclear receptor-coactivator interactions. Genes Dev 12:3343-56

20. Collingwood TN, Wagner R, Matthews CH, Clifton-Bligh RJ, Gurnell M, Rajanayagam O, Agostini M, Fletterick RJ, Beck-Peccoz P, Reinhardt W, Binder G, Ranke MB, Hermus A, Hesch RD, Lazarus J, Newrick P, Parfitt V, Raggatt P, de Zegher F, Chatterjee VK 1998 A role for helix 3 of the TRbeta ligand-binding domain in coactivator recruitment identified by characterization of a third cluster of mutations in resistance to thyroid hormone. EMBO J 17:4760-70

21. Feng W, Ribeiro RC, Wagner RL, Nguyen H, Apriletti JW, Fletterick RJ, Baxter JD, Kushner PJ, West BL 1998 Hormone-dependent coactivator binding to a hydrophobic cleft on nuclear receptors. Science 280:1747-9

22. Yagi H, Pohlenz J, Hayashi Y, Sakurai A, Refetoff S 1997 Resistance to thyroid hormone caused by two mutant thyroid hormone receptors beta, R243Q and R243W, with marked impairment of function that cannot be explained by altered in vitro 3,5,3'-triiodothyroinine binding affinity. J Clin Endocrinol Metab 82:1608-14

23. Safer JD, Cohen RN, Hollenberg AN, Wondisford FE 1998 Defective release of corepressor by hinge mutants of the thyroid hormone receptor found in patients with resistance to thyroid hormone. J Biol Chem 273:30175-82

24. Wagner R, Huber B, Shiau A, Kelly A, Cunha-lima ST, Scanlan T, Apriletti J, Baxter JD, West BL, Fletterick RJ 2001 Hormone Selectivity in Thyroid Hormone Receptors. 15:398-410

25. Richards FM, Kundrot CE 1988 Identification of structural motifs from protein coordinate data: secondary structure and first-level supersecondary structure. Proteins 3:71-84

26. Pissios P, Tzameli I, Kushner PJ, Moore DD 2000 Dynamic Stabilization of Nuclear Receptor Ligand Binding Domains by Hormone or Corepressor Binding. 6:245-253

27. Behr M, Loos U 1992 A point mutation (Ala229 to Thr) in the hinge domain of the c-erbA beta thyroid hormone receptor gene in a family with generalized thyroid hormone resistance. Mol Endocrinol 6:1119-26

28. Onigata K, Yagi H, Sakurai A, Nagashima T, Nomura Y, Nagashima K, Hashizume K, Morikawa A 1995 A novel point mutation (R243Q) in exon 7 of the c-erbA beta thyroid hormone receptor gene in a family with resistance to thyroid hormone. Thyroid 5:355-8

29. Johnson BA, Wilson EM, Li Y, Moller DE, Smith RG, Zhou G 2000 Ligand-Induced Stabilization of PPARγ Monitoured by NMR Spectroscopy: Implications for Nuclear Receptor Activation. 298:187-194

30.   Horlein AJ, Naar AM, Heinzel T, Torchia J, Gloss B, Kurokawa R, Ryan A, Kamei Y, Soderstrom M, Glass CK, Rosenfeld MG 1995 Ligand-independent repression by the thyroid hormone receptor mediated by a nuclear receptor corepressor. 377:397-404

31.   Apriletti JW, Baxter JD, Lau KH, West BL 1995 Expression of the rat alpha 1 thyroid hormone receptor ligand binding domain in Escherichia coli and the use of a ligand-induced conformation change as a method for its purification to homogeneity. Protein Expr Purif 6:363-70

32.   Otwinowski Z, Minor W 1997 Processing of x-ray diffraction data collected in oscillation mode. 276:307-326

33.   Brunger AT, Adams PD, Clore GM, DeLano WL, Gros P, W. G-KR, Jiang JS, Kuszewski J, Nilges M, S. PN, Read RJ, Rice LM, Simonson T, Warren GL 1998 Crystallography and NMR system: a new software suite for macromolecular structural determination. Acta Crystallogr D 24:905-921

34.   4 CCPN 1994 The CCP4 suite: programs for protein crystallography. Acta Crystallogr D 50:760-763

## Introduction

Steriodogenic factor one (SF-1) is an orphan nuclear receptor responsible for the activation of genes involved in mammalian sexual differentiation and endocrine organogenesis. The SF-1 nuclear receptor is encoded by the Ftz-F1 gene. In mice the disruption of this gene prevents the formation of adrenals, gonads and ventromeidal hypothalamus as well as selected pituitary cell types (1-4) A recently discovered human patient with one defective copy of SF-1 displayed sex reversal and adrenal insufficiency(5). SF-1 was originally identified as a nuclear receptor (NR) from its characteristic DNA binding Domain (DBD) sequence. However, arrangement of the SF-1 receptor is different than most of the other members of the nuclear receptors. The activation function one (AF-1) domain is located adjacent to the ligand-binding domain (LBD). In most other NR's this domain is located prior to the DBD. Following the AF-1 domain is a truncated LBD, which starts at helix two rather than helix one. Helix one has been replaced with an uncharacteristically long proline rich hinge domain, which links the LBD to the DBD. This unusual arrangement localizes both the LBD and AF-1 in one continuous sequence.

The existence of a hormone for SF-1 has not been demonstrated. One potential ligand, 25-hydroxycholesterol, activates SF-1 in CV-1 cells, but fails to activate in any other cell line (6-8). The apparent lack of a cognate ligand may be the result of rapid degradation of the ligand or the ligand may be a ubiquitous molecule. Clearly, an X-ray crystal structure would help to determine whether SF-1 has a ligand and aid in identification of the ligand if one is present. Most evidence suggests that this receptor is activated by phosphorylation rather than ligand binding and may lack a cognate hormone. Studies of SF-1 activation have found that phosphorylation of Ser 203 strongly enhances transcription from SF-1 controlled

genes (9). Phosphorylation is mediated by the MAP kinase Erk2. The Erk2 signaling pathway responds to signals originating from cell surface receptors under the control of peptide-hormone signals such as GnRH, FSH and ACTH. This is consistent with observation that cell surface receptors can activate SF-1 controlled genes (10-13).

SF-1 may be part of a new structural class of NR's that respond primarily to MAP kinase signaling or they may have a yet undiscovered hormone. In either case the structure SF-1 would expand our understanding of the interactions between the LBD and AF-1 domains. Such a structure would also show how phosphorylation regulates nuclear receptors.

## Materials and Methods

### SF-1 Expression and purification[1]

SF-1 constructs $SF-1_{178-462}$ and $SF-1_{219-462}$ were produced by PCR from the full length cDNA clone, subcloned in plasmid pBH4[2] and expressed in E.coli BL21(DE3)pLysS (Novagen) with yields of soluble protein 20-30 mg per liter of culture when grown at 25°C. When expressed in plasmid pBH4, the protein acquires HisX6 tag followed by tobacco etch virus (TEV) protease cleavage site. Initial purification steps include the affinity column for the His-tag (TALON© Pharmacia) and digestion with TEV protease. Final purification step is monoQ column (Pharmacia). Mono Q A buffer included 20 mM tris-HCl pH 7.6, 5mM DTT, 2 mM CHAPS, I mM EDTA, and B buffer had 1 M NaCl, in addition[3].

---

[1] This protocol was designed in collaboration with I. Krylova under the supervision of H. Ingraham, UCSF
[2] A gift from Dr. W. Lim, UCSF
[3] Protein was received from the Ingraham lab at this stage of purification

## Mass Spectrometry

SF-1 samples were analyzed with mass spectroscopy to assess purity. All mass spectra of purified SF-1 were obtained with a Voyager DE MALDI TOF[4] mass spectrometer using the factory-preset method for bovine serum albumin (BSA). Prior to analysis SF-1 containing solutions were purified and desalted with a Ziptip C-18 (Milipore) using the standard protocol. Sinapinic acid matrix solution was prepared daily using the following protocol: 60% acetonitrile, 39% water, 0.3% TFA[5] and 10mg/ml of fresh Sinapinic Acid (Sigma). Approximately 1ul of sinapinic acid matrix was placed on a stainless steel target plate (Perceptive Biosystems) for each protein sample. An equal volume of SF-1 was mixed with the sinapinic acid matrix and allowed to dry under a fan until no moisture remained. These samples were then analyzed with the Voyager DE instrument

## DLS Protocol

SF-1 protein was generally kept at concentrations near 6.5mg/ml to avoid rapid aggregation that occurred at higher concentrations. Buffer exchange for DLS experiments was accomplished with three dilution/concentration steps with the test buffer solution. During the concentration step protein concentration was not allowed to exceed 6.5mg/ml. At each dilution step the protein was mixed thoroughly. After the final concentration step the protein solution was spun at 45K for thirty minutes in a Ti 45 rotor to remove particulate. The solution was passed through a 0.1 micron filter and placed in a 45μl quartz cuvette (Protein Solutions). DLS measurements were take with a DynaPro DLS (Protein Solutions). Data was analyzed using the DynaPro software package

---

[4] Matrix assisted laser desorption ionization (MALDI) time of flight (TOF)
[5] Trifluoroacetic acid

## Proteolysis for Mass Spectrometry

A protocol developed by Kanaani et al. was followed to determine the locations of reactive cystines. This method uses mass spectrometry to identify the location of reactive cystines. Peptide fragments obtained from trypsin or chymotrypsin digestion of SF-1 were desalted with C-18 Ziptips using the standard protocol. Matrix solutions were prepared using the same recipe stated previously, except both α-Cyano acid and Sinapinic acid were used as matrices.

## Thermal Unfolding Observed with Circular Dichroism

Sample of SF-1 were prepared for CD by diluting the protein solution from 6.5 mg/ml to 0.25 mg/ml with CD buffer (150mM NaCl and 50mM Tris pH 8.0). The samples were prepared and maintained at 4 C until analysis. Thermal unfolding was performed on a Jasco 1029 CD system equipped with a temperature controller. A temperature ramp from 4 C to 90 C at 0.5 C/min was used to unfold SF-1.

# Results

## Analysis of Initial SF-1$_{178-462}$ Construct

The initial construct of SF-1 consisted of residues 178-462, which contained the phosphorylation site of SF-1. This protein had been purified as describe in the methods section. The SDS Page gel of this protein indicated that the protein was very pure and was not generally clipped by the TEV protease. However, further analysis of this protein with nondenaturing gels and mass spectrometry indicated that the protein was heterogeneous and formed multimers in solution.

## Purification of SF-1$_{178-462}$

The first column used for further purification was the MonoQ column. The SF-1 protein would elute from the column in two peaks. The first peak proved to be heterogeneous, like the starting material. The second peak was primarily monomeric on a nondenaturing gel and also showed fewer multimers with mass spectrometry. However this material would quickly precipitate. Aggregation was confirmed both with nondenaturing gels and dynamic light scattering, which showed that the multimeric species became more populated over time.

## Cystine Identification and Removal

An Iodoacetylation time course was used to determine the number of reactive cystines in SF-1$_{178-462}$ (see figure 3-1) This experiment showed that three cystines were highly reactive and would become acetylated within 90 minutes. Three other cystines would react as the reaction went to completion, which took approximately ten hours. Thus of the eight cystines in our construct three of them were highly reactive, three were slightly reactive and two more were nonreactive. This result was confirmed with Nbs$_2$, which produces a quantitative fluorescent signal at 412nm once reacted with cystine. Though this technique went to completion in five minutes the result indicated that six cystines were reactive and approximately three cystines were highly reactive.

The sites of the cystines were mapped using a combination of iodoacetylation and protolytic digestion. Iodoacetylation of SF-1 was performed for 90 minutes. Both tryptic and chymotryptic digestion was used to provide redundancy of data. Both acetylated and native protein was subjected to protolysis. Peptide fragments that contained added acetates shifted in the mass spectrum. These fragments were pieced together to determine the

position of the reactive cystines. The results indicated that four cystines in SF-1 reacted with iodoacetate. These were Cys 202, 248, 267 and 423. The positions the reactive cystines are shown in figure 3-2. Three of the reactive Cys residues 202, 267 and 423 were mutated to Ser.

## Analysis of the SF-1$_{217-462}$ Construct

The longer construct SF-1$_{178-462}$ had aggregation problems even after the three highly reactive cystines were removed. Optimizing the buffer to stabilize SF-1 had almost no effect on the longer construct. At this point our efforts shifted to a different construct of SF-1. A shorter construct of SF-1, which contained residues 217-462, was analyzed to determine if it was a good candidate for crystallization. This protein was purified in the same way as the longer construct. However, both peaks collected from the MonoQ Column appeared to be identical biochemically. Since it was impossible to tell which peak was the right peak to work with, we worked with both peaks.

Analysis of the construct with SDS Page and nondenaturing gels indicated that the protein was monomeric, which was confirmed with both DLS and mass spectrometry. DLS results were obtained by putting the protein through a filter prior to analysis. This technique confirmed that the protein was monomeric immediately after purification and concentration. Unfortunately, filtration would remove a significant portion of the protein from solution on the days subsequent to purification, indicating that SF-1 multimers had formed and could not pass through the filter pores.

## Crystallization Trials

The quality of SF-1 protein gradually increased as optimizations were made to the purification protocol. Protein quality improvements can be seen in figure 3-3. Each protein construct and purification method would give rise to a set of crystallization trial. These trials consisted of screening SF-1 with the Hampton #1 and Hampton #2 (Hampton Research) as well as Wizard #1 and Wizard #2 (Emerald Bioscience) factorial crystallization screens. Any promising conditions from these screens would be followed up with grid screens. In our initial crystal screens we used a protein concentration of ~9mg/ml, later this concentration was reduced to 6.5mg/ml to minimize aggregation. Concentrations of 1.5 mg/ml, 3 mg/ml and 4.5 mg/ml were also screened. Generally drops were set up with a 1:1 and 2:1 ratio of protein solution to well solution. Certain factors appeared in all of the screens to stabilize SF-1. These were moderate concentrations of NaCl (50-300mM). Small amounts of MPD ~5% or glycerol ~15%. High pH (pH > 8.0) as well as very low pH (pH < 4.0) tended to stabilize SF-1. However, no diffracting crystals were obtained though crystalline material was found frequently in MPD conditions with the shorter construct.

## Discussion

### Smaller Construct is More Stable

Our results would suggest that the SF-1 protein was not particularly stable. We have

made significant improvements in obtaining stable protein, especially in the shorter SF-1$_{217-}$

$_{462}$ construct, but there is still work to be done. Clearly the hinge segment of SF-1 plays a

key role in stability. The longer SF-1$_{178-462}$ construct, which possesses the hinge segment,

was less stable and rapidly aggregated. We have been unable to obtain sufficient quantities

of phosphorylated SF-1$_{178-462}$ to determine if this is a stabilizing factor. Elimination of the

hinge significantly increased the stability of SF-1. This suggests that the hinge of SF-1 is not

providing a significant number of stabilizing interactions to the LBD and is probably highly

mobile. The proline richness and phosphorylation site of the hinge would suggest that this

region would be exposed to other regulatory proteins.

### Successes and Failures

The primary success of these experiments was the isolation of a stable construct of

SF-1. Combining the shorter construct of SF-1$_{217-462}$ with the M3C mutation in optimized

buffer conditions resulted in a protein that was far more stabile than the SF-1$_{178-462}$ construct.

The SF-1$_{217-462}$ M3C construct would remain clear for many days in the optimized buffer

solution. Once the protein did start to aggregate it would appear as a white precipitate rather

than as a yellow or light brown precipitate that was observed with the SF-1$_{178-462}$ construct.

The SF-1$_{217-462}$ construct also worked well for NMR studies, while the SF-1$_{178-462}$ construct

gave a smeared out signal that was uninterpretable. However, the shorter construct lacks the

phosphorylation site and is a less desirable target for crystallization.

## Future Direction

Both of the M3C constructs had the same three cystines removed those were 202, 267 and 423. However, one cystine identified by mass spectrometry as highly reactive was present in both constructs. The cystine at position 248 was identified in both the tryptic and chymotryptic digest as being modified by iodoacetate during the 60-minute conjugation. This residue may have caused the aggregation observed in the M3C constructs. Stabilization of either construct of SF-1 required at least 15mM DTT or 5mM TCEP. These concentrations are significantly higher than the concentration normally required to maintain cystines in the reduced state. Elimination of this highly reactive cystine may aid in stabilizing the protein and eventually in crystallization. The initial iodoacetylation time course showed that six of the eight cystines found in SF-1 were reactive when the iodoacetylation was carried to completion. The use of reducing agents could be enough to keep the remaining less reactive cystines reduced. However, these two cystines could also be removed once identified, or all of the cystines could be removed to avoid the identification process.

The removal of cystines alone may not prevent the aggregation of the SF-1 protein. Clearly the SF-1$_{217-462}$ M3C construct is more stable than the SF-1$_{178-462}$ M3C construct. The long hinge region containing the phosphorylation site appears to play a part in the aggregation process as demonstrated in both DLS and NMR experiments. This segment of SF-1 is rich in Pro residues and also contains a large number of hydrophobic residues. Making a series of constructs differing in length by two to four residues from residue 178-202 may allow the identification of a stable construct, which contains the phosphorylation site at Ser 203. Another possibility is to screen a number of different organisms to find a

construct of SF-1 that is stable enough for crystallization. This may be difficult because SF-1 contains a significant number of cystines in most species. It may be necessary to make cystineless mutants of all of these SF-1 constructs as well.

Phosphorylation of the protein may also stabilize the Pro rich hinge domain presumably by making it more hydrophillic. It has proven difficult to phosphorylate SF-1 experimentally because of the equilibrium between the phosphorylated and unphosphorylated form of SF-1. Separation of these two species is difficult and the yields are low.

Finding a ligand or molecule that stabilizes SF-1 may also provide a path to crystallization. This would require a great deal of screening and would be better left to a drug company or collaborator with a sizable drug library. However, Circular Dichroism would provide a good method of screening molecules for stabilization of SF-1.

# References

1.  Ingraham HA, Lala DS, Ikeda Y, Luo X, Shen WH, Nachtigal MW, Abbud R, Nilson JH, Parker KL 1994 The nuclear receptor steroidogenic factor 1 acts at multiple levels of the reproductive axis. Genes Dev 8:2302-12

2.  Luo X, Ikeda Y, Parker KL 1994 A cell-specific nuclear receptor is essential for adrenal and gonadal development and sexual differentiation. 481-490

3.  Sadovsky Y, Crawford PA, Woodson KG, Polish JA, Clements MA, Tourtellotte LM, Simburger K, Milbrandt J 1995 Mice deficient in the orphan receptor steroidogenic factor 1 lack adrenal glands and gonads but express P450 side-chain-cleavage enzyme in the placenta and have normal embryonic serum levels of corticosteroids. Proc Natl Acad Sci U S A 92:10939-43

4.  Shinoda K, Lei H, Yoshii H, Nomura M, Nagano M, Shiba H, Sasaki H, Osawa Y, Ninomiya Y, Niwa O, et al. 1995 Developmental defects of the ventromedial hypothalamic nucleus and pituitary gonadotroph in the Ftz-F1 disrupted mice. Dev Dyn 204:22-9

5.  Achermann JC, Ito M, Hindmarsh PC, Jameson JL 1999 A mutation in the gene encoding steroidogenic factor-1 causes XY sex reversal and adrenal failure in humans [letter]. Nat Genet 22:125-6

6.  Christenson LK, McAllister JM, Martin KO, Javitt NB, Osborne TF, Strauss JF, 3rd 1998 Oxysterol regulation of steroidogenic acute regulatory protein gene expression. Structural specificity and transcriptional and posttranscriptional actions. J Biol Chem 273:30729-35

7. Lala DS, Syka PM, Lazarchik SB, Mangelsdorf DJ, Parker KL, Heyman RA 1997 Activation of the orphan nuclear receptor steroidogenic factor 1 by oxysterols. Proc Natl Acad Sci U S A 94:4895-900

8. Mellon SH, Bair SR 1998 25-Hydroxycholesterol is not a ligand for the orphan nuclear receptor steroidogenic factor-1 (SF-1). Endocrinology 139:3026-9

9. Hammer GD, Krylova I, Zhang Y, Darimont BD, Simpson K, Weigel NL, Ingraham HA 1999 Phosphorylation of the nuclear receptor SF-1 modulates cofactor recruitment: integration of hormone signaling in reproduction and stress. Mol Cell 3:521-6

10. Kaiser UB, Conn P, Chin WW 1997 Studies of gonadotropin-releasing hormone (GnRH) action using GnRH receptor expressing cell lines. 18:46-70

11. Liu Z, Simpson ER 1997 Steroidogenic factor 1 (SF-1) and SP1 are required for regulation of bovine CYP11A gene expression in bovine luteal cells and adrenal Y1 cells. Mol Endocrinol 11:127-37

12. Sugawara T, Holt JA, Kiriakidou M, Strauss JF, 3rd 1996 Steroidogenic factor 1-dependent promoter activity of the human steroidogenic acute regulatory protein (StAR) gene. Biochemistry 35:9052-9

13. Wilson TE, Fahrner TJ, Milbrandt J 1993 The orphan receptors NGFI-B and steroidogenic factor 1 establish monomer binding as a third paradigm of nuclear receptor-DNA interaction. Mol Cell Biol 13:5794-804
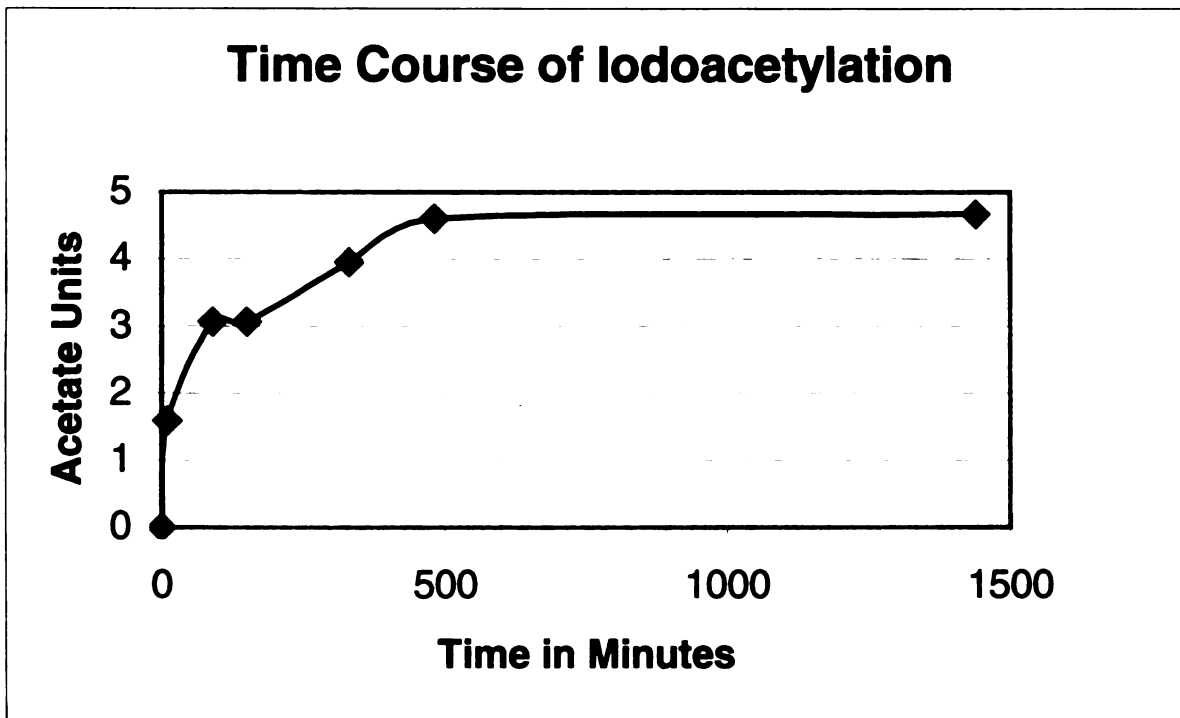
# Time Course of Iodoacetylation



**Figure 3-1: Time Course of Iodoacetylation of SF-1**

The degree of Iodoacetylation of SF-1 was monitored by mass spectroscopy. Increase in SF-1 mass was divided by expected increase per acetate modification to determine the number of acetate units added to SF-1. Clearly there are two plateaus. The first plateau occurs at three acetate units after 90 minutes of reaction. Full acetylation of SF-1 takes many hours and two Cys residues remain unmodified

**1**

AGYLYPAFSNRTIKSEYPEPYASPPQQPGPPYSYPEPFSGGPN⬛⬛⬛QLEPE⬛

**2** ⬛⬛⬛LQEPAKSRSDQ **3** ⬛⬛⬛C⬛⬛R⬛MVFKELE⬛ **4**

**5** ⬛C⬛⬛YRQVQYGKEDSILLVTGQEVELS⬛⬛GSLL **6** ⬛⬛ **7**

**8** ⬛LQLD⬛C⬛LFSLDVKFLN⬛⬛ **9** C⬛YPHCG⬛ **10**
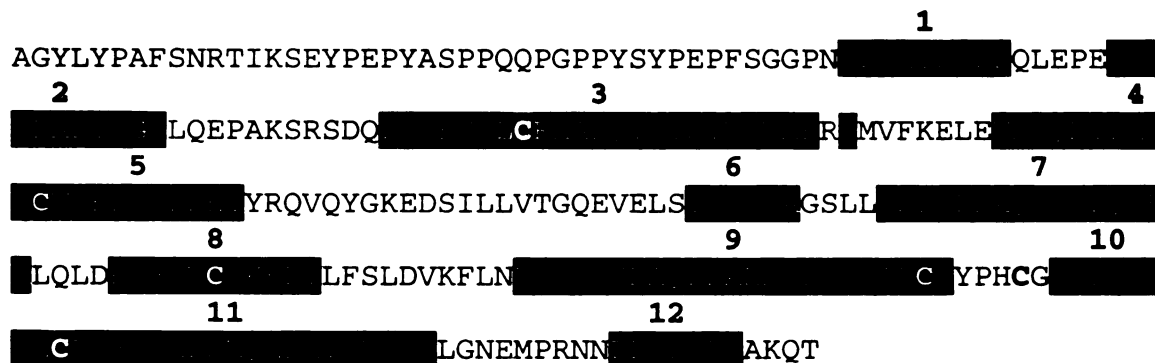
**11** ⬛C⬛⬛LGNEMPRNN **12** ⬛⬛AKQT

## Figure 3-2: Positions of the reactive cystines

Proteolytic fragments of SF-1 were analyzed by mass spectroscopy. Peptide fragments containing acetate modifications displayed increased mass. The positions of the modified cystines were mapped to primary sequence of SF-1. The four highly reactive cystines that were modified during the ninety-minute incubation are shown in red. Those regions of the receptor that are thought to be helical are black inverse. A total of six cystine were modified when the reaction when to completion. The locations of the two moderately reactive cystines were not determined with this experiment.
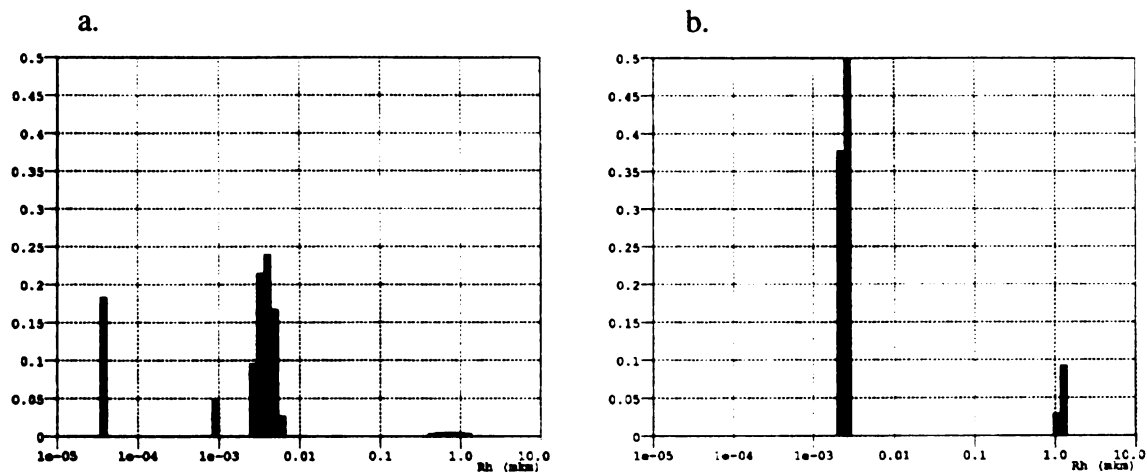
**Figure 3-3: Comparison of initial SF-1$_{217-462}$ DLS profile with a more recent sample**

DLS profiles of SF-1 were taken at the beginning of the project and more recently, after three

cystines had been removed and the purification protocol had been optimized. a. The SF-1$_{217-}$

$_{462}$ protein was analyzed with DLS revealing significant aggregation as well as a broad

distribution of molecular weights. This type of profile is not optimal for crystallography. b.

The SF-1$_{217-462}$ M3C mutant in stabilization buffer. Some higher order aggregates are

observed. Overall, this protein sample has a smaller average mass and a tighter distribution

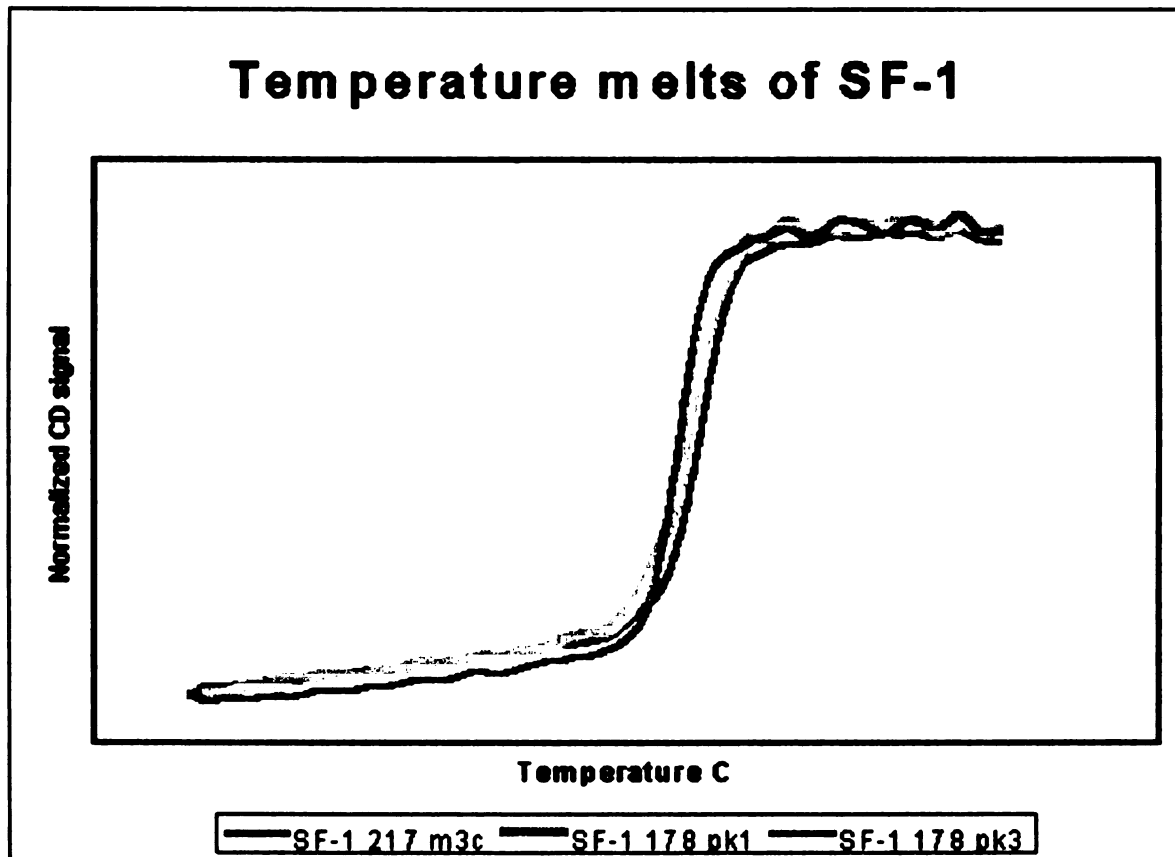of masses. This is a much better profile for protein crystallography

**Temperature melts of SF-1**

Normalized CD signal

Temperature C

SF-1 217 m3c     SF-1 178 pk1     SF-1 178 pk3

**Figure 3-4: Temperature melts of Different SF-1 Constructs**

Circular Dichroism was used to monitor the thermal denaturation of a number of SF-1

proteins used for crystallization trials. SF-1 is primarily $\alpha$-helical and thermal transitions can

be follow at $UV_{222}$. The smaller $SF-1_{217}$ was the most thermally stable. There is a small

difference in thermal stability between peak 1 and peak 2 of the longer construct, with peak

one being more stabile.